Determination of Multiquantum Vibrational Transition Moments in Hydrogen Iodide and Their Significance in its Vibrational Photochemistry

by

Robert H. Reiner

In Partial Fulfillment of the Requirements
for the Degree of
Master of Science

California Institute of Technology
Pasadena, California 91125

1976

(Submitted December 18, 1975)

ACKNOWLEDGMENTS

This thesis is dedicated to my parents, Mary and Bob, for their many years of sacrifice on my behalf.

Professor Aron Kuppermann has been the principal investigator in this research and I thank him for his support. I would also like to thank George Schatz, Jackie Berg, and Tom Orlowski for their friendship and professional interaction during the course of this research.

ABSTRACT

Estimates of the band intensities of transitions between the ground and upper vibrational levels (1-9) were made for HI. Calculations were performed with both Morse and RKR oscillator wavefunctions, using various functional approximations for the dipole operator fitted to known experimental results. Absorption measurements using a multiple pass cell placed upper bounds on transition intensities, which were not inconsistent with the calculated values. (Band strengths for HI $\Delta v = 8,9$ are less than 5×10^{-4} cm^{-2} atm^{-1}.)

The feasibility of using these multiquantum vibrational transitions to pump the reaction

$$HI + HI^*(v = 8,9) \rightarrow H_2 + 2I$$

is discussed.

TABLE OF CONTENTS

I. Introduction

The availability of high intensity, tunable dye lasers has created a renewed interest in visible and near UV photochemistry (300-800 nm). In addition to studying the photochemistry of molecules with low lying electronic states, the availability of an intense, very monochromatic light source in this region could conceivably use "forbidden" multi-quantum rotational, vibrational transitions to populate upper vibrational levels of the ground electronic state, allowing one to study the effect of vibrational energy on chemical reactions. Indeed, photochemistry of this type has been done, using a chemical laser to excite an "allowed" transition in HCl.[1]

The best choice for such a molecule would be a diatomic. This would simplify problems of intramolecular energy transfer after an excited rotation vibration state is produced, making the kinetics tractable. Since the intensity of a vibrational transition decreases markedly as Δv (the change in vibrational quantum number) increases, the vibrational spacing should be large so that Δv can be kept small when attempting to pump a reaction involving this molecule with visible light. Finally, the activation energy for a bimolecular reaction involving it should be sufficiently small for the added vibrational energy to be a significant fraction of the activation energy.

Hydrogen iodide was chosen with the above considerations in mind. The fundamental band absorption is observed at ~2300 cm^{-1}. Observation of the first, second, and third vibrational overtones indicates that

absorption of visible light would correspond to transitions in which $\Delta v = 7,8$ or 9.[2] The 0→8 absorption corresponds to approximately 45 kcal/mole of vibrational energy. The activation energy for the reaction

$$HI + HI \rightarrow H_2 + 2I \qquad (A)$$

is 44 kcal/mole.[3,4]

If it is possible to produce a significant steady state population of HI*(v = 7, 8 or 9), then one could study the vibrationally excited analog of reaction A,

$$HI^* + HI \rightarrow H_2 + 2I \qquad (B)$$

The feasibility of observing reaction B depends on the magnitude of the transition moment, $\langle 8|M(R)|0\rangle$, where M(R) is the dipole operator as a function of internuclear distance, R.

Calculations and experiments performed to measure this moment are presented. The feasibility of studying reaction B in bulk gas phase is then discussed, and results of preliminary attempts for measuring its rate are presented.

II. THEORY

The strength, $S_{v,J,M}^{v',J',M'}$, of a vibrational transition between states v and v', produced by interaction of an electromagnetic field with a molecule, can be shown (by time-dependent perturbation theory) to be proportional to the square of the transition moment.[5,6] That is,

$$S_{v,J,M}^{v',J',M'} \propto |\langle v,J,M|\underset{\sim}{\mu}|v',J',M'\rangle|^2$$

$$\equiv \left|\int \Psi^*_{v,J,M}(\underset{\sim}{R},\underset{\sim}{r})\underset{\sim}{\mu}(\underset{\sim}{R},\underset{\sim}{r})\Psi_{v',J'M'}(\underset{\sim}{R},\underset{\sim}{r})d\tau\right|^2, \qquad (1)$$

where quantum numbers J and M specify the rotational angular momentum and its projection on the laboratory z axis. Since eigenfunctions $\Psi_{v,J,M}(\underset{\sim}{R},\underset{\sim}{r})$ and $\Psi_{v',J',M'}(\underset{\sim}{R},\underset{\sim}{r})$ are functions of nuclear and electronic coordinates, the integration specified in Eq. (1) must be performed over both sets of coordinates ($d\tau = d\underset{\sim}{R}d\underset{\sim}{r}$).[6]

In the Born-Oppenheimer approximation, the electronic motion is assumed to be independent of nuclear motion; this means $\Psi_{v,J,M}(\underset{\sim}{R},\underset{\sim}{r})$ may be separated into a product of a pure electronic wavefunction $U_R(\underset{\sim}{r})$ and a nuclear wavefunction

$$\chi_{v,J,M}(\underset{\sim}{R}); \qquad \Psi_{v,J,M}(\underset{\sim}{R},\underset{\sim}{r}) = V_R(\underset{\sim}{r})\chi_{v,J,M}(\underset{\sim}{R}).$$

$\chi_{v,J,M}(\underset{\sim}{R})$ is written as

$$\chi_{v,J,M}(\underset{\sim}{R}) = (1/R)\psi_{v,J}(R)Y_{J,M}(\theta,\phi), \qquad (2)$$

a product of a spherical harmonic $Y_{J,M}(\theta,\phi)$, whose arguments refer to the orientation of R with the laboratory axes, and $\psi_{v,J}(R)$ a solution to the radial Schrödinger equation

$$\frac{d^2\psi_{v,J}(R)}{dR^2} + \frac{2m}{\hbar^2}\{E - V(R) - \frac{\hbar^2 J(J+1)}{2mR^2}\}\psi_{v,J}(R) = 0. \quad (3)$$

In Eq. (3), V(R) is the mechanical potential, J is the rotational quantum number, and m is the reduced mass.[7] Similar statements hold for $\psi_{v',J',M'}(\underset{\sim}{R},\underset{\sim}{r})$.

In a diatomic molecule, the dipole moment, $\underset{\sim}{\mu}$, must be directed along the internuclear axis. From Eqs. (1), (2), and the Born-Oppenheimer approximation we get

$$\langle v,J,M|\underset{\sim}{\mu}|v',J',M'\rangle \propto \int \chi^*_{v,J,M}(\underset{\sim}{R})\underset{\sim}{M}(R)\chi_{v',J',M'}(\underset{\sim}{R})d\underset{\sim}{R} \quad (4)$$

$$\propto \int \psi^*_{v,J}(R)M(R)\psi_{v',J'}(R)dR \int Y^*_{J,M}(\theta,\phi) \times \hat{\underset{\sim}{R}} Y_{J',M'}(\theta,\phi)d\Omega \quad (5)$$

$$\propto \langle v,J|M(R)|v',J'\rangle\langle J,M|\hat{\underset{\sim}{R}}|J',M'\rangle, \quad (6)$$

[8]

where

$$\underset{\sim}{M}(R) \equiv \int U^*_R(\underset{\sim}{r})\underset{\sim}{\mu}(R,\underset{\sim}{r})U_R(\underset{\sim}{r})d\underset{\sim}{r} = M(R)\hat{\underset{\sim}{R}}. \quad (7)$$

When Eq. (6) is squared, summed over all M′, and averaged over all M, the intensity of a particular rotational line, $S^{v',J'}_{v,J}$, is obtained. The total band strength, $S^{v'}_{v}$, of a vibrational transition between states v and v′ is defined as the sum of the intensities of all rotational vibrational transitions in the band and is denoted by $S(v \rightarrow v')$ or simply S. Therefore, knowledge of M(R) and the nuclear radial wavefunction $\psi_{v,J}(R)$ suffice to evaluate S.

If V(R) is known, Eq. (3) can be integrated to give $\psi_{v,J}(R)$. Band strengths may then be computed using Eq. (7) and an assumed form of M(R).

Rather than compute wavefunctions and transition moments for each rotational state in the vibrational band, we assume that in the rotational term in Eq.(3), R can be replaced by its equilibrium value for J = 0. The corresponding $\psi_{v,J}(R)$ is then essentially independent of J and the total nuclear energy becomes the sum of vibrational and rotational energies with no vibrational rotational coupling.

This simplification is a very good approximation. Herman and Wallis[9] have shown that this approximation introduces into the J^{th} rotational transition moment a relative error of order $J \cdot B_e/\omega_e$, where B_e is the rotational constant at equilibrium nuclear separation, and ω_e is the vibrational constant at equilibrium position. For HI, $B_e/\omega_e \approx 0.003$. Calculations performed on the first three vibrational bands showed that this simplification produced less than 10% error in HI band strengths. Since this is much less than the error produced by extrapolation of M(R) to transitions of higher Δv, this simplification is entirely justified.

Computation of transition moments becomes a straightforward problem of determining eigenfunctions of the potential, V(R), which are then used in Eq.(7) to evaluate $\langle v | M(R) | v' \rangle$ for a particular choice of M(R).

III. Calculation of Band Strengths

A. Potential Energy Curves

One of the spectroscopic problems with the hydrogen halides is the absence of a low lying bound electronic state which emits to the ground state.[10] As a result, emission spectra cannot be used to determine the energies of all the vibrational eigenstates. Hence, the RKR method cannot be used to generate a complete potential energy curve (as, for example, has been done for Na_2).[11]

Instead, using ω_e, $\omega_e x_e$, $\omega_e y_e$, $\omega_e z_e$ determined from absorption experiments,[2,12] the positions of the first eleven eigenstates were calculated. They are listed in Table I. The RKR procedure of Demitröder, McClintock, and Zare[11] was then used to determine the classical turning points for each calculated eigenvalue. The smoothed potential curve drawn through these points using a cubic spline method is shown in Figure 1.

For comparison, the HI Morse potential was used. The parameters listed in Table II were used to construct the Morse curve also shown in Figure 1.[13] While both curves agree near the bottom of the well, above v=3 they begin to diverge. This is not unexpected, since it is well known that the Morse potential fails to describe the molecule accurately near the dissociation limit.[14] The RKR potential may not be exact either, even if the eigenvalues used to generate it are exact, since a potential which reproduces the energy levels of a molecule is not unique.[15] However, as shown later, use of either potential below v=10

Table I. Eigenvalues of HI(cm^{-1}).

v	Calculated from spectroscopic data*	Integration of Morse Potential	Integration of RKR Potential
0	1144.59	1140.90	1144.04
1	3374.17	3344.70	3372.86
2	5523.86	5480.64	5519.62
3	7592.63	7439.43	7584.13
4	9579.31	9331.24	9565.15
5	11482.20	11119.42	11463.02
6	13299.22	12804.35	13275.39
7	15027.93	14386.84	15001.45
8	16665.48	15866.10	16641.21
9	18208.63	17242.92	18193.06

* See reference 2.

Table II. Morse Parameters for HI.

$$V(R) \equiv D_e(1 - e^{-\beta(R-R_e)})^2$$

$$\text{where } \beta \equiv 1.2177 \times 10^7 \, \omega_e \sqrt{\frac{\mu_A}{D_e}}$$

For HI

$D_e = 25843.41 \text{ cm}^{-1}$

$R_e = 3.04069 \text{ bohr}$

$\beta = 0.92520 \text{ bohr}^{-1}$

Figure 1. HI potential energy, V(R), is plotted as a function of internuclear separation, R. The Morse parameters are listed in Table II. RKR turning points shown in solid circles, ●. Eigenvalues are shown for each potential as well as the first five Morse eigenfunctions.

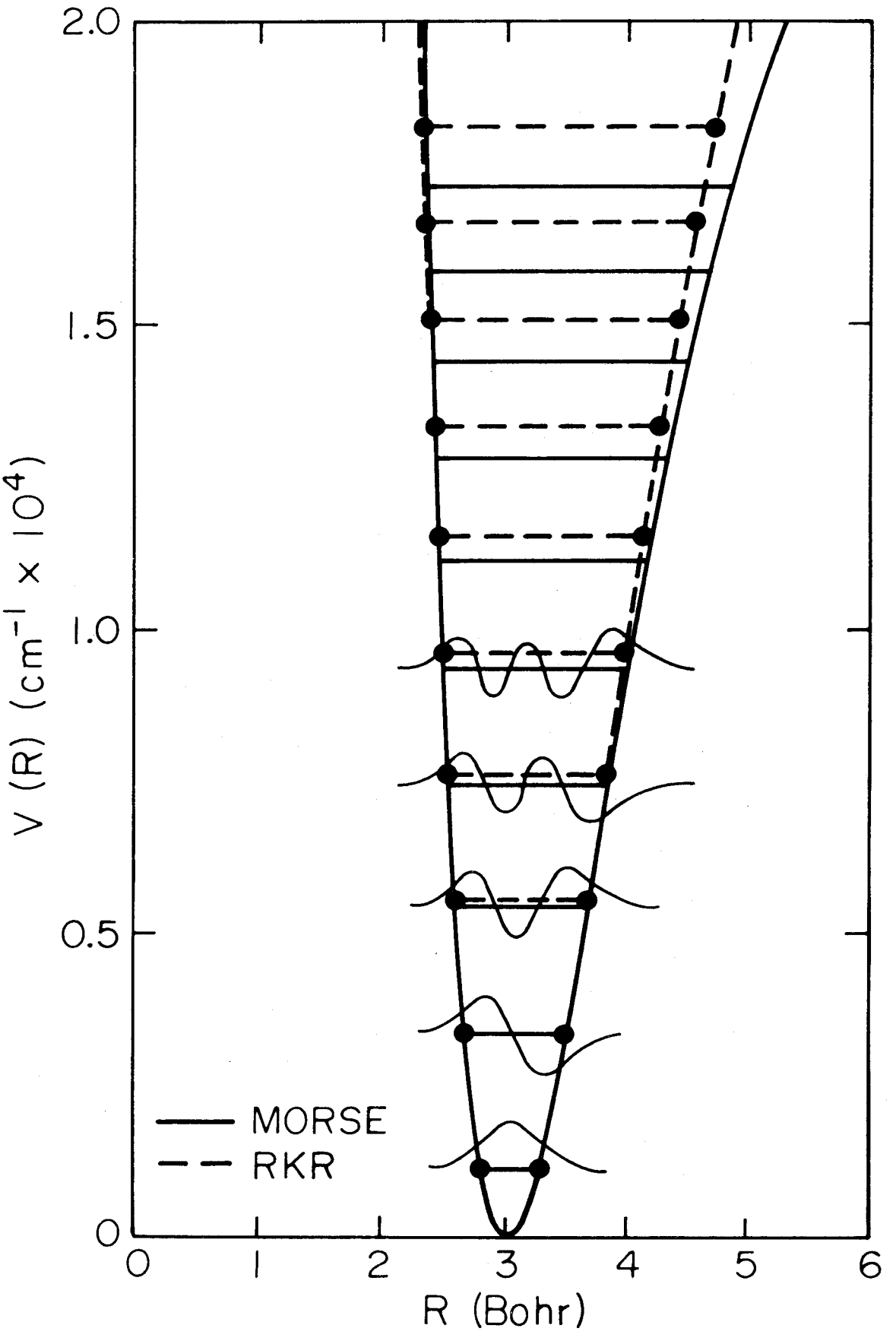
2.0
1.5
1.0
0.5
0
V (R) (cm^{-1} x 10^4)
0
1
2
3
4
5
6
R (Bohr)
MORSE
RKR

is justified in this work, because the error in approximating the dipole moment operator exceeds the difference between calculations using the different potentials.

B. Wavefunctions

Equation 3 is integrated for both potentials by the finite difference method. The resulting matrix equations are solved using the Givens-Householder method.[16] Eigenvalues calculated in this manner are shown for both potentials in Figure 1 along with some Morse eigenfunctions. The integration procedure was checked by comparing the eigenvalues used to generate the RKR potential with those calculated from equation 3 using that potential. As shown in Table I, they agree to within 0.2 percent.

C. Dipole Moment Operator

Determination of M(R) as a function of internuclear distance R is the greatest source of error in the band strength calculation. We have fitted several trial functions, $\tilde{M}(R)$, to measured band intensities. Other band strengths are then calculated using this $\tilde{M}(R)$ and compared.

First we attempted to approximate M(R) by

$$M(R) \simeq \tilde{M}(R) = A \cdot R e^{-B \cdot R} \qquad (8)$$

Equation 8 satisfies the necessary boundary conditions

$$\tilde{M}(0) = 0 \tag{9}$$

and

$$\tilde{M}(\infty) = 0 \tag{10}$$

However, when A and B were adjusted to yield the measured fundamental[17] and first overtone[18] intensities, a third condition,

$$\langle 0|\tilde{M}(R)|0\rangle = M_0^0 \quad , \tag{11}$$

where M_0^0 is the permanent dipole moment, was not met.

We next tried an operator of the form

$$M(R) \approx \tilde{M}(R) = AR^n e^{-BR} \tag{12}$$

where A,B and n were fitting parameters. When A,B and n were adjusted to give curve A in Figure 2 (chosen to match the leading coefficients in the Taylor series expansion of M(R) about R_e--see below), a disappointing fit to experimental results was observed (see Figure 3, curve A).

Better results are obtained by expanding the dipole operator in a Taylor series about R_e, the equilibrium internuclear separation,

$$M(R) = M_0 + M_1(R-R_e) + M_2(R-R_e)^2 + \ldots \tag{13}$$

In this treatment, equation 13 is truncated at the appropriate order, M_0 is approximated by M_0^0 and the remaining coefficients are expressed in terms of the fundamental and higher order band strengths. This yields a set of linear equations.[19] Since the measured intensities are related

Table IIIa. Dipole Moment Operator Approximations, $\tilde{M}(R)$.

Trial (Fig. 2-6)	Potential	Form $\tilde{M}(R)$	i_{max} for M_i polynomial	$M_0{}^3$	$M_0{}^4$	Equation
A	Morse	Exponential	----	---	---	12
B	Morse	Polynomial	2	---	---	13
C	Morse	Polynomial	2	---	---	13
D	Morse	Polynomial	3	+	---	13
E	Morse	Polynomial	3	-	---	13
F	Morse	Polynomial	4	+	+	13
G	Morse	Polynomial	4	+	-	13
H	Morse	Polynomial	4	-	+	13
I	Morse	Polynomial	4	-	-	13
J	Morse	Polynomial	4	(Average F-I)		13
K	Morse/RKR	Pade	----	+	---	16
L	RKR	Polynomial	2	---	---	13
M	RKR	Polynomial	3	+	---	13
N	RKR	Polynomial	3	-	---	13

Table IIIb. Dipole Moment Operator Approximations, $\tilde{M}(R)$

Trial	Equation	Constants (a.u.) M_0	M_1	M_2	M_3	M_4
A	12	(A = 0.1880, B = 0.3188, n = 0.7958)				
B	13	0.1654	-0.01067	0.0175	----	----
C	13	0.1654	-0.01071	0.0155	----	----
D	13	0.1654	0.006943	0.02862	-0.01807	----
E	13	0.1654	0.002230	0.008325	0.05860	----
F	13	0.1654	0.007110	0.02797	-0.02113	0.006603
G	13	0.1654	0.003901	0.03787	0.02677	-0.09777
H	13	0.1654	0.005853	-0.003004	0.003916	0.1192
I	13	0.1654	0.002645	0.006897	0.05182	0.01478
J	13	0.1654		(Average of F - I)		
K	16	0.1654	(A = 0.0268, B = -0.1194, C = -0.9446, D = 0.3541, E = -0.6823)			
L	13	0.1654	0.006197	0.02354	----	----
M	13	0.1654	0.007287	0.02749	-0.01675	----
N	13	0.1654	0.002475	0.009963	0.05761	----

Figure 2. Various approximations of the dipole operator, M(R), are plotted as functions of internuclear distance, R. Curve labels, O, refer to Table III.

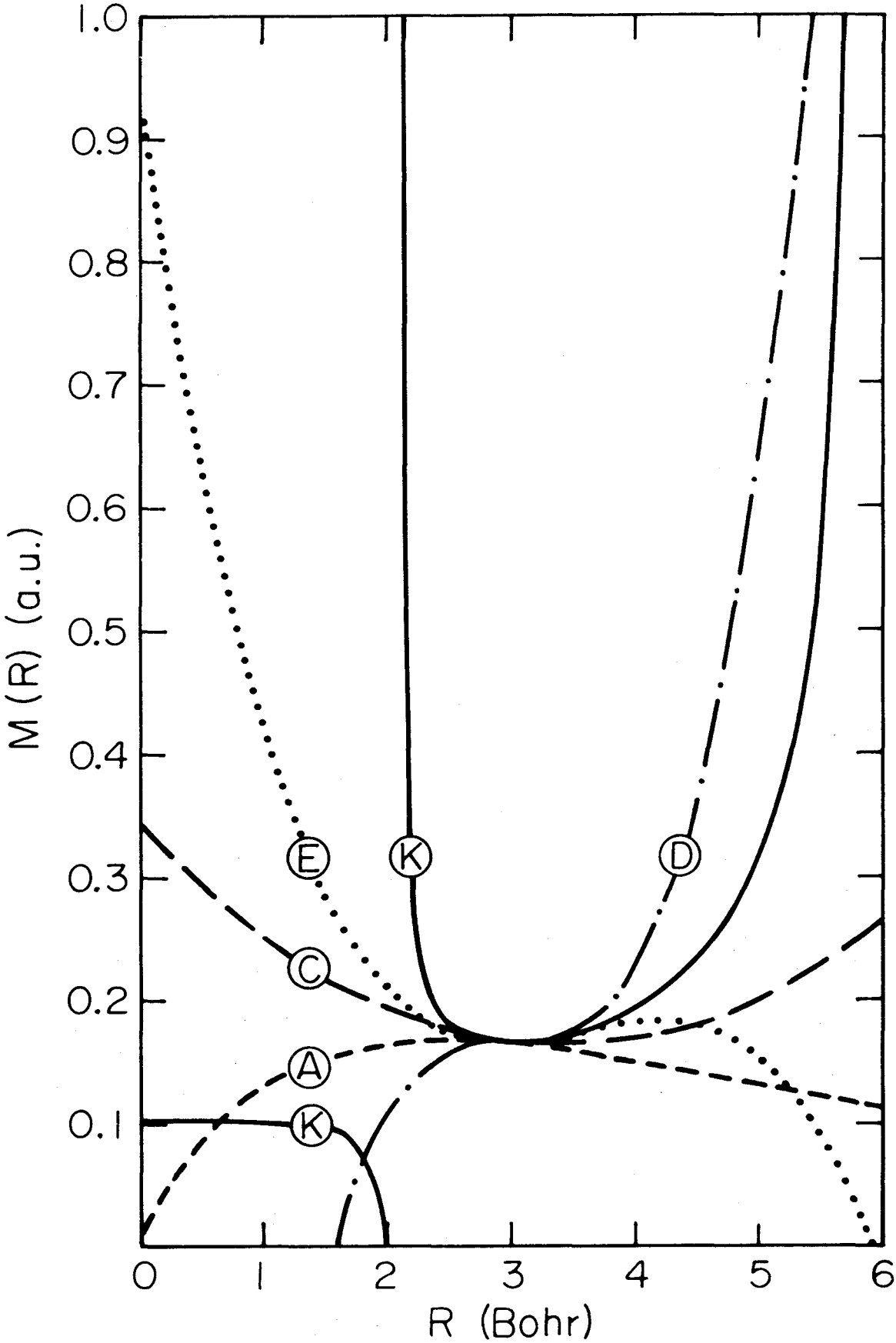
1.0
0.9
0.8
0.7
0.6
0.5
0.4
0.3
0.2
0.1
M (R) (a.u.)
0
1
2
3
4
5
6
R (Bohr)
E
K
D
C
A
K

Figure 3. Total band strength, S, is plotted versus change in vibrational quantum number, Δv, for Morse oscillator transitions from the ground vibrational state to state v. Curves A , B , and C are calculations described in text and Table III. Solid circles, ● , are experimental results and approximations explained in text. Bars shown for $\Delta v = 8$ and 9 are experimentally established upper bounds for S.

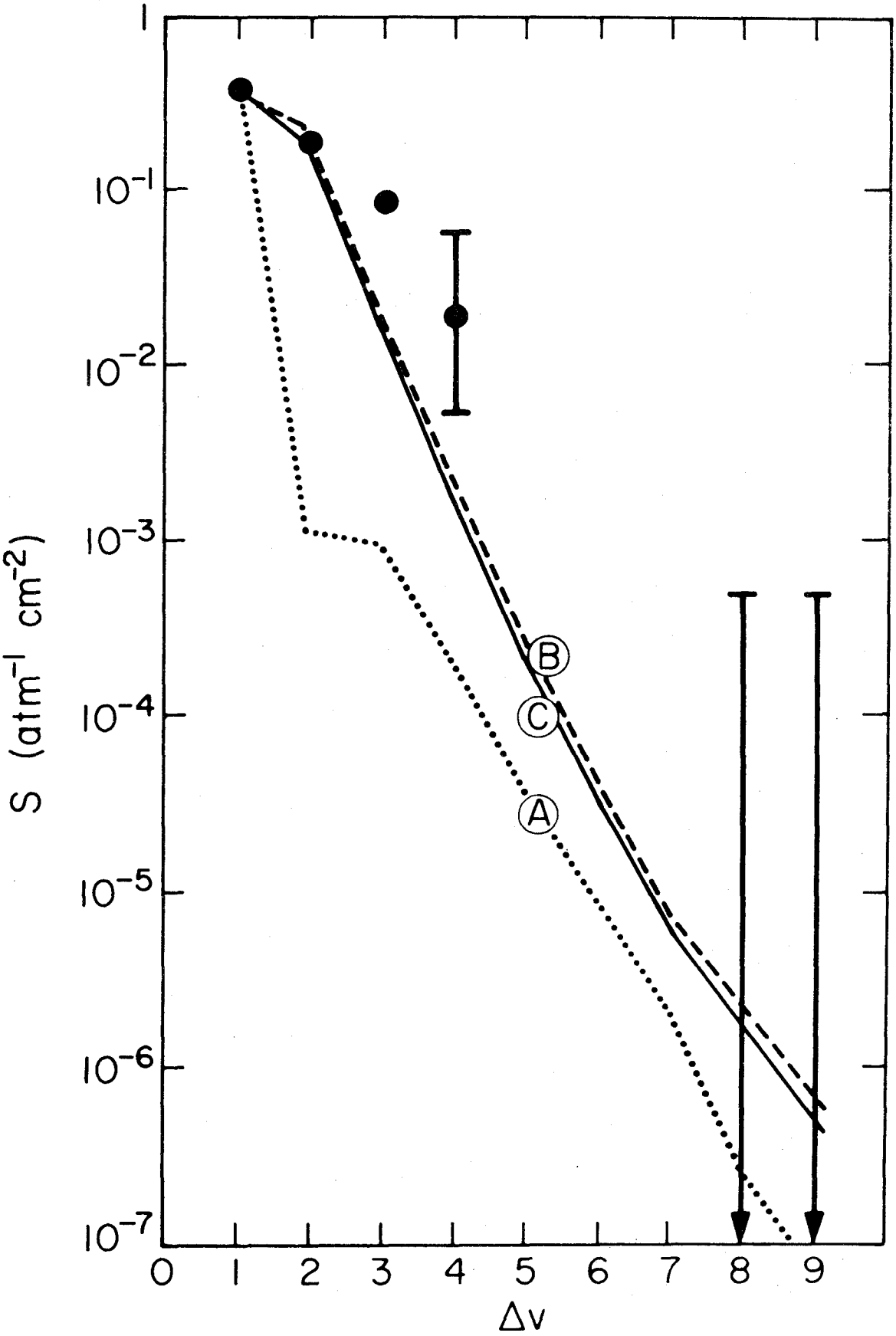
1
10^{-1}
10^{-2}
10^{-3}
10^{-4}
10^{-5}
10^{-6}
10^{-7}
S (atm^{-1} cm^{-2})
0 1 2 3 4 5 6 7 8 9
Δv
A
B
C

to the square of the matrix elements, there exists an ambiguity in the sign of the higher order moments, which can be resolved by measurement of the individual rotation lines in each band.[20]

Benesch has used this method to analyze data on the fundamental and first overtone.[18] Curve B in Figure 3 was obtained using Benesch's values for M_1 and M_2 (higher terms in equation 13 being omitted) and the Morse potential wavefunctions. It slightly overestimates the first overtone intensity. This is not unexpected since his operator was optimized for a different potential,

$$V(R) = F(R-R_e)^2 - G(R-R_e)^3 \qquad (14)$$

The fortuitous agreement of curve B with experimental results is, in fact, only because Benesch's potential, equation 14, and the Morse potential are identical about R_e.

Choosing coefficients M_1 and M_2 which give proper fundamental and first overtone band intensities for the Morse potential, one gets curve C in Figure 3. M_1 and M_2 so obtained are well within the experimental uncertainty proposed by Benesch. As seen in Figure 3, the curves are in good agreement, even when extrapolated to $\Delta v = 9$.

The danger of using this type of approximation for the dipole operator in computing transitions beyond the data base is discussed by Truschka and Salwen.[21] The truncation of a Taylor series expansion of any function about R_e becomes a poorer approximation to the function as $(R-R_e)$ becomes larger. This is clearly seen in Figure 2 where several

polynomial approximations are plotted as functions of internuclear separation. When an nth order polynomial is found which fits the first n transition moments, the approximations agree quite well for small Δr,

$$\Delta r \equiv |R - R_e| \tag{15}$$

As Δr increases, however, the various approximations diverge. Unfortunately, successively higher transitions "sample" the dipole operator at larger Δr.

From experimental data on the 0→3 transition,[22] two cubic polynomial approximations are generated (curves D and E in Figure 4) depending on the sign of $M_0^3 \equiv \langle 0|M(R)|3\rangle$. The quadratic polynomial underestimates the 0→3 band intensity by an order of magnitude. Yet, the quadratic and cubic polynomials do not differ by more than that when extrapolated to $\Delta v = 9$.

Using the experimental conditions given by Haeusler and Meyer[12] to make an order of magnitude estimate of $|M_0^4|$, four quartic approximations of M(R) are computed (curves F, G, H, I in Figure 5). Since the approximation of $|M_0^4|$ is crude, and since the signs of M_0^3 and M_0^4 are not known, perhaps it is better to compare the quadratic and cubic approximations of M(R) with the average of all the quartic results (curve J). Not surprisingly, as the order of the polynomial approximation increases, the calculated curves begin to converge.

Herbelin and Emanuel[20] have suggested using a Pade approximation for the dipole moment operator,

$$\tilde{M}(R) = \frac{A(R-R_e)^2 + B(R-R_e) + C \cdot M_0}{D(R-R_e)^2 + E(R-R_e) + C} \tag{16}$$

Figure 4. Total band strength, S, is plotted versus change in vibrational quantum number, Δv, for Morse oscillator transitions from the ground vibrational state to state v. Curve labels, O, are described in text and Table III.

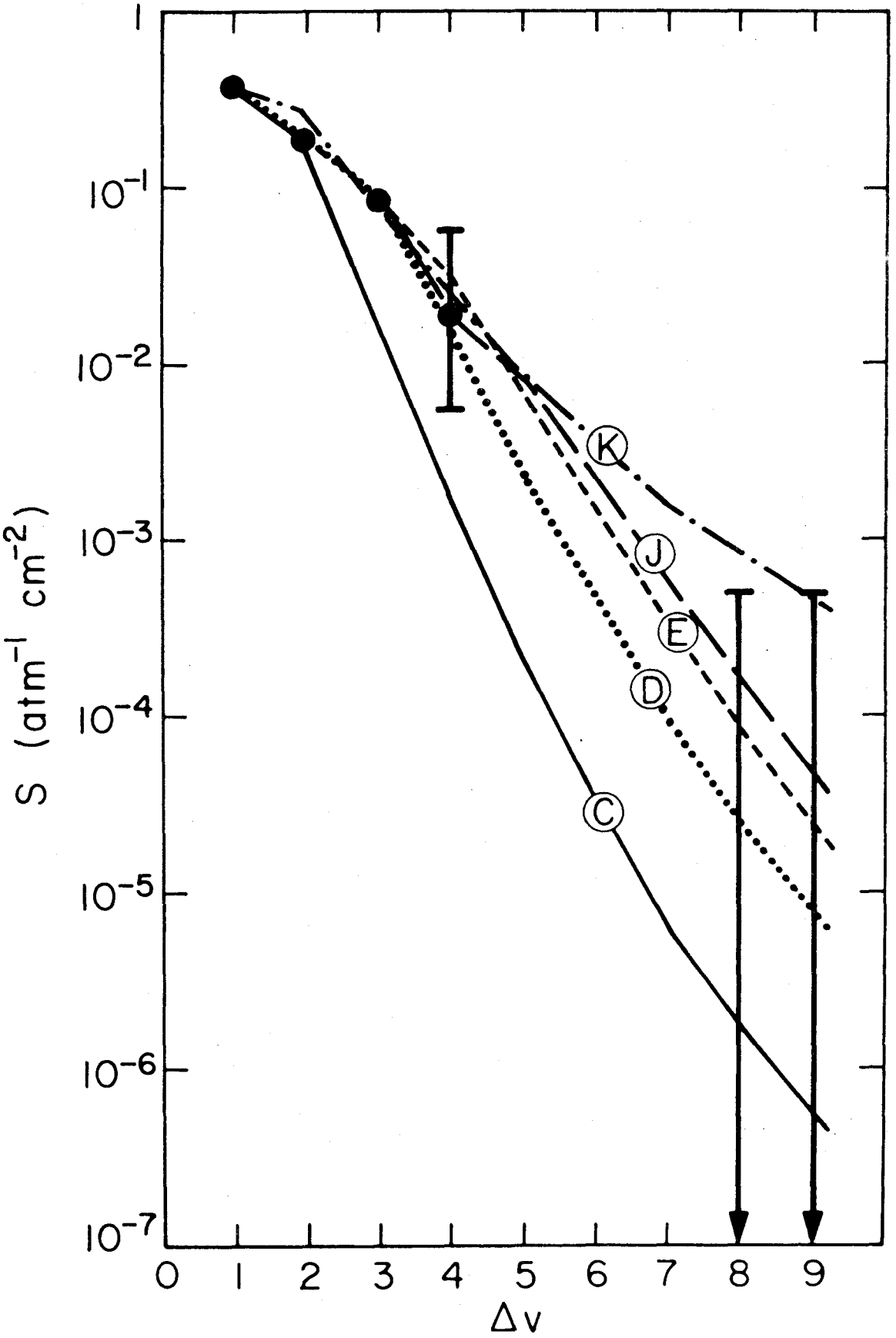
1
10^{-1}
10^{-2}
10^{-3}
10^{-4}
10^{-5}
10^{-6}
10^{-7}
S (atm^{-1} cm^{-2})
0 1 2 3 4 5 6 7 8 9
Δv
K
J
E
D
C

Figure 5. Total band strength, S, is plotted versus change in vibrational quantum number, Δv, for Morse oscillator transitions from the ground vibrational state to state v. Curve labels, O, are described in text and Table III.

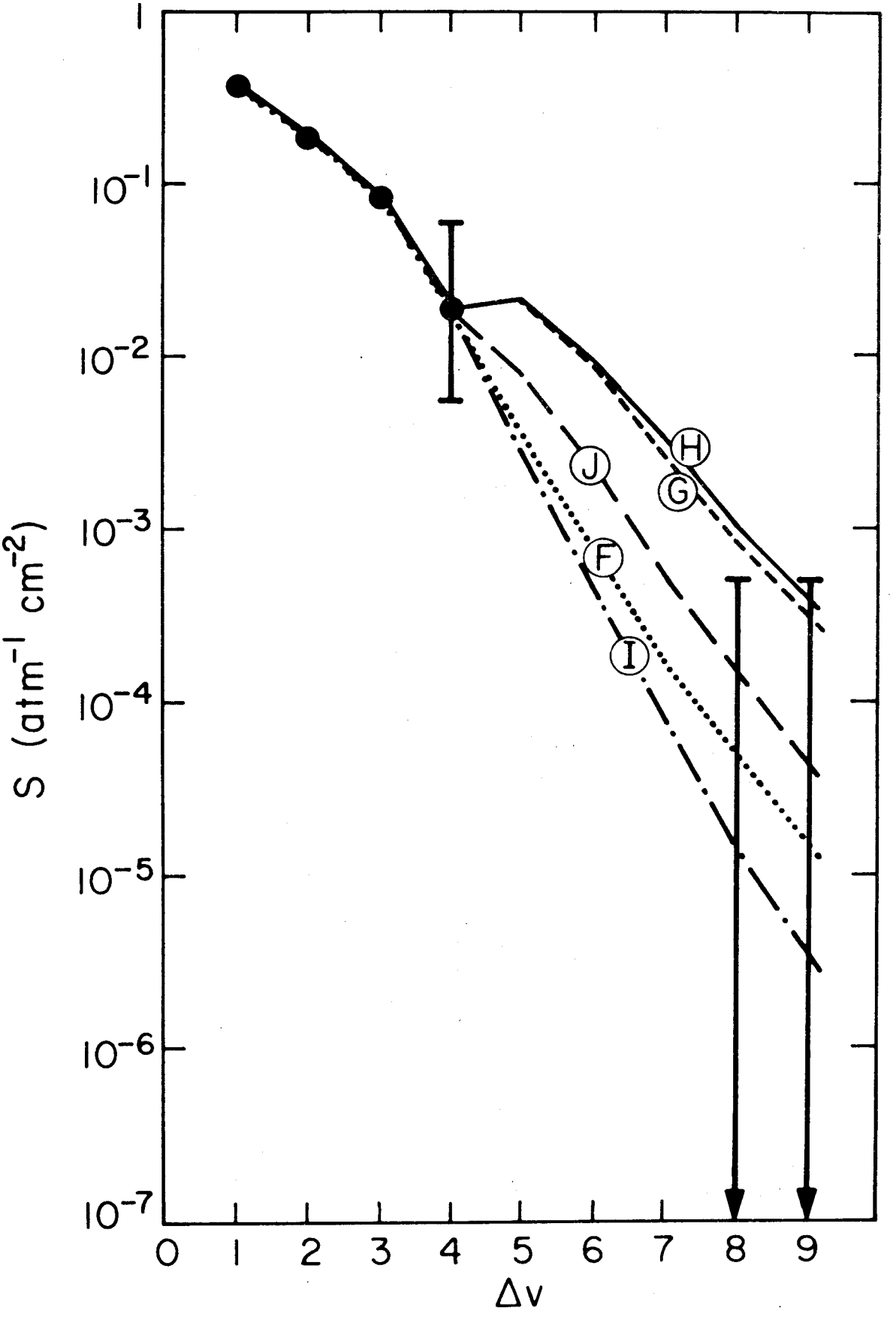
1
10^{-1}
10^{-2}
10^{-3}
10^{-4}
10^{-5}
10^{-6}
10^{-7}
S (atm^{-1} cm^{-2})
0 1 2 3 4 5 6 7 8 9
Δv
H
G
J
F
I

where the coefficients A, B, C, D, and E are known functions of the polynomial coefficients used in equation 13. Herbelin and Emanuel have shown that for HF, the Pade approximation gives better agreement with experiment than a cubic polynomial for transitions outside the data base of the polynomial. Presumably, the Pade approximation behaves more like M(R) than does the cubic approximation for large Δr. However, one should note that the Pade approximation puts an unphysical singularity in the dipole curve at 2 bohr (Figure 2). Evidently, one must still use caution when extrapolating the Pade results to higher Δv.

Curve K of Figure 4 shows the band intensities predicted by the Pade method. While only data from the fundamental, first and second overtones determine curve K, note that the Pade method predicts the third overtone strength previously guessed.[12]

Up to this point, only results for the Morse potential solutions of equation 3 have been discussed. Figure 6 compares band intensities calculated from Morse and RKR eigenfunctions. It is apparent that the form of the HI potential is not as critical as the form of the dipole operator.[22] Indeed, the Pade results are identical for both potentials, and even for the quadratic polynomial, the intensities agree when $\Delta v \leq 6$. While it is true that the form of the potential may change the calculated band strengths for large Δv, it seems unproductive to search for better representations of V(R) until more information about M(R) becomes available.

Figure 6. Total band strength calculations using the Morse potential are compared to calculations using the RKR potential. See Table III.

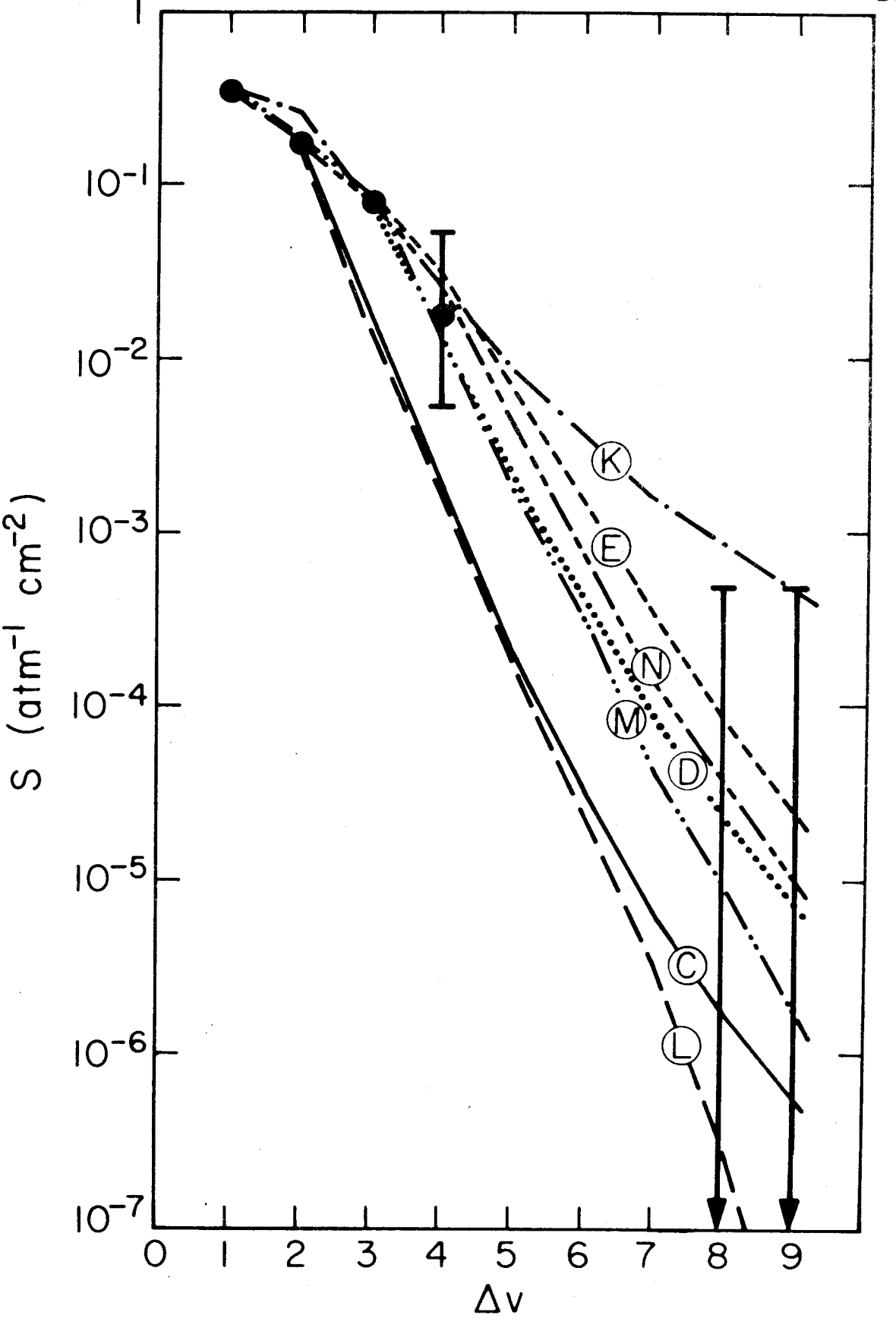
1
10^{-1}
10^{-2}
10^{-3}
10^{-4}
10^{-5}
10^{-6}
10^{-7}
S (atm^{-1} cm^{-2})
0 1 2 3 4 5 6 7 8 9
Δv
K
E
N
M
D
C
L

IV. Experimental Determination of Band Intensities

The experimental measurement of weak optical transitions using a multiple pass or White cell is a well documented, thirty-year-old procedure.[23] Herzberg, for example, was able to obtain an equivalent path length of 55 km atmospheres while looking at the quadrupole allowed rotation-vibration spectrum of hydrogen.[24] However, at the two to three atmosphere pressures necessary in this experiment, HI proved to be too corrosive for the mirrors to be mounted inside the multipass cell. This necessitated our modification of the method developed by White and Herzberg to locate weak transitions in non-corrosive gases.[25]

The simple act of moving the mirrors outside the multiple pass cell complicates the experimental procedure enormously. Since the light must pass through two windows on each traversal of the cell, the reflective losses at the window surfaces are large. For the 1.5 cm thick plate glass windows used on our cell, reflective losses were 0.17 per traversal. In a 40 pass experiment, the incident intensity, I_0 , is reduced by,

$$\frac{I}{I_0} = (1 - 0.17)^{40} = 6.3 \times 10^{-4} \quad , \qquad (17)$$

more than three orders of magnitude compared to a multiple pass cell with mirrors inside. Attempts to find a protective mirror coating that would allow mirrors to be mounted inside the cell were not successful.

The apparatus used to measure line strengths consisted of three components: (1) a source of tunable monochromatic radiation; (2) the multiple pass cell; (3) a detection system. A schematic is shown in

Figure 7.

A tunable dye laser (Coherent Radiation 490), pumped by a CW argon ion laser (Spectra Physics 170), was used as a monochromatic light source. The argon laser supplied a maximum of eighteen watts input power to the dye laser. The dye laser produced a well-collimated, two to four watt beam with a 0.05 nm bandwidth (FWHM). The dye laser wavelength drive was calibrated using a 1.83 meter scanning spectrometer (Jarrel-Ash 78-400). The beam was chopped at 40 hz and focused by a 50 cm F.L. lens upon mirror A of the multiple pass cell.

The multipass cell consisted of two spherical mirrors, placed outside a 144 cm long, 15 cm diameter absorption cell. The mirrors (A and B in Figure 7) were 150 cm radius of curvature, 15 cm diameter, spherical, front surface, silvered mirrors arranged as suggested by Bernstein and Herzberg.[25] Mirror A was fixed, while split mirror B could be rotated to change the number of traversals. Without the absorption cell in place, a maximum of 164 traversals between A and B were obtained, corresponding to an optical path of 246 meters. With the absorption cell in place, scattered and reflected light limited the number of cell traversals to 32 before the signal at photodiode P was too weak to be detected.

The chopped signal at silicon PIN photodiode, P, (United Detector Technology 6DP) was normalized to that of reference diode R and processed by a lock-in amplifier (P.A.R., HR-8). The output of the amplifier was recorded as the dye laser was scanned from 660 nm to 560 nm.

Hydrogen iodide (Matheson Gas Products, 98% purity) was vacuum distilled three times from an acetone slush bath (180 K), the center one

Figure 7. Schematic diagram of the experimental apparatus used to measure weak transitions.

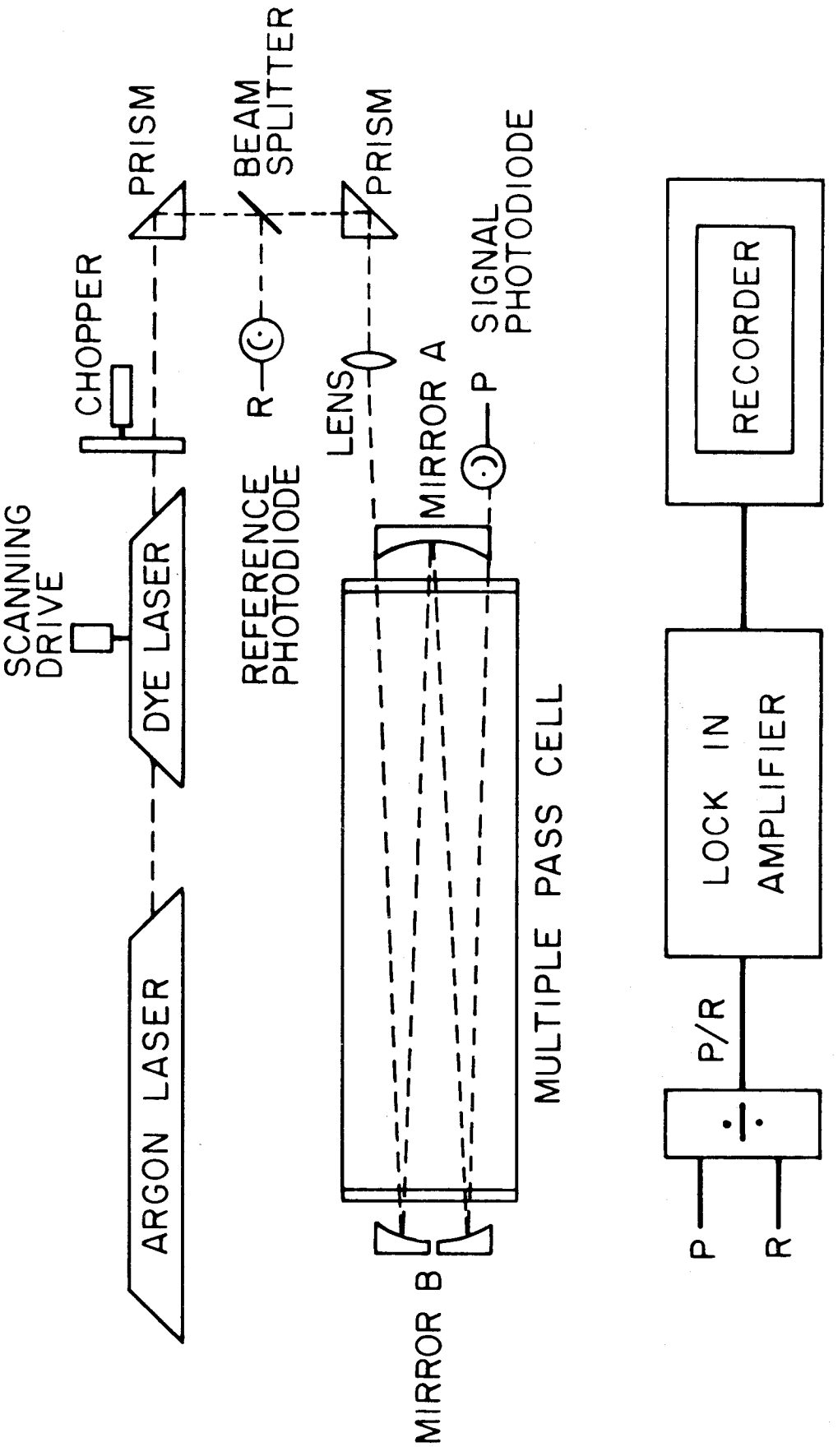
ARGON LASER
DYE LASER
SCANNING DRIVE
CHOPPER
PRISM
BEAM SPLITTER
REFERENCE PHOTODIODE
R
LENS
PRISM
MIRROR A
P
SIGNAL PHOTODIODE
MULTIPLE PASS CELL
MIRROR B
P/R
LOCK IN AMPLIFIER
RECORDER
P
R

third being retained after each distillation. Between two and three atmospheres of HI were added to the cell. A cold trap on the absorption cell was maintained at 263 K to remove any I_2 formed from HI photolysis or reactions with stopcock grease.

V. Results

No absorption (100% transmission ±5% noise) was observed for an effective path length of 90 meter atmospheres. This placed an upper limit of 5.0×10^{-4} atm^{-1} cm^{-2} on the total band intensities of the $\Delta v = 8$ and 9 transitions shown in Figures 3-6. An upper limit on the line strength of the strongest rotational vibrational transition in either band is 5×10^{-5} atm^{-1} cm^{-2}.

Curves J and K in Figure 4 form upper and lower bounds for the band strengths for $\Delta v \leq 9$. The median of J and K may be the best estimate of the band strengths. This agrees with all experimental band strength for $\Delta v \leq 4$ and is not inconsistent with the experimental upper bounds set for $\Delta v = 8,9$. Therefore, the value

$$S_{0\rightarrow 8} \leq 5 \times 10^{-4} \text{ atm}^{-1} \text{ cm}^{-2}$$

is used in our discussion of HI vibrational photochemistry.

VI. Discussion

The feasibility of using a multiquantum vibrational transition $HI(v = 0 \rightarrow 8)$ to pump reaction B in the gas phase is now considered. Suppose a vessel of HI is irradiated with an intense laser beam, producing absorption from the ground state to the eighth vibrational level in an attempt to observe reaction B. It is important to note that observation of increased reaction rate in the photolyzed sample (above that in a thermal one) is a necessary but not a sufficient indication of rate enhancement due to vibrational excitation[26] (see Appendix I). Indeed, a detailed analysis of the reaction kinetics is necessary to determine the effect of vibrational excitation.

Assume the following mechanism describes the above experiment:

$$HI + h\nu \rightarrow HI^*(v = 8) \qquad (C)$$

$$HI^* + HI \rightarrow HI(v < 8) + HI \qquad (D)$$

$$HI^* + HI \rightarrow H_2 + 2I \qquad (B)$$

$$HI + HI \rightarrow H_2 + 2I \qquad (A)$$

Making the steady state approximation on $\{HI^*\}$, one obtains

$$\{HI^*\}_{ss} = \frac{I_0 \cdot \varepsilon_{HI} \cdot \ell}{k_B + k_D} \qquad (18)$$

where ℓ is the absorption path length, ε_{HI} is the extinction coefficient for the pumped transition $(0,J \rightarrow 8,J')$ k_B and k_D are the rate constants

for reaction B and reaction D. Using reaction A, reaction B, and equation 18, the rate of H_2 formation is

$$\text{Rate}_{H_2} = \frac{I_0 \varepsilon_{HI} \ell k_B \{HI\}}{k_D + k_B} + k_A \{HI\}^2 \quad . \tag{19}$$

Two important facts are displayed in equation 18 and equation 19. First, $\{HI^*\}_{ss}$ is pressure independent. This means that reaction A and reaction B obey different rate laws, reaction A is second order while reaction B is first order. The contributions of each reaction may be separated (see Appendix I). Second, the contribution of reaction B in equation 19,

$$\text{Rate}_B = \frac{I_0 \varepsilon_{HI} \ell k_B \{HI\}}{k_D + k_B} \tag{20}$$

not only depends on laboratory parameters ($I_0, \ell, \{HI\}$) and k_B and ε_{HI}, as anticipated, but also on k_D (the relaxation process).

Thus, information concerning k_D is vital in the analysis of equation 20. In general, the measured first order rate constant in equation 19 is proportional to $k_B/k_B + k_D$. That is,

$$\text{Rate}_{H_2} = C \cdot \frac{k_B}{k_B + k_D} \{HI\} + k_A \{HI\}^2 \tag{21}$$

where $C = I_0 \varepsilon_{HI} \ell$. If, for example, $k_B >> k_D$, equation 20 reduces to

$$\text{Rate}_{B(k_B >> k_D)} \approx I_0 \varepsilon_{HI} \ell \{HI\} \tag{22}$$

Under conditions of equation 22, the measured rate is independent of k_B, making the proposed experiment meaningless.

Equation 20 cannot be used to solve $Rate_B$ for k_B since k_D is not known. There are, in fact, several processes by which the vibrationally excited HI molecule can relax to the ground vibrational state. Thus k_D is a weighted average of the rate constants for each of those processes. The processes include infrared fluorescence, collisional deactivation via vibrational to translational energy transfer (V→T) and collisional deactivation via vibrational to vibrational energy transfer (V→V).

If one assumes that the most important deactivation step in reaction D is

$$HI^*(v=8) + HI(v=0) \rightarrow HI(v=7) + HI(v=1) \quad , \qquad (E)$$

the following approximation may be made:

$$k_D \approx k_E \quad . \qquad (23)$$

Justification for equation 23 is based on two assumptions:

a) At pressures used to perform the photochemistry ({HI}>5 torr), infrared fluorescence can be neglected. Using the Einstein coefficient of HI(v=1)

$$A_{0\leftarrow 1} = 0.038\ sec^{-1} \quad ,^{27} \qquad (24)$$

with the assumption that the radiative lifetime of HI(v=8), τ_8, is the same order of magnitude as τ_1,[28]

$$\tau_1 \sim \tau_8 \quad , \qquad (25)$$

one finds that

$$\tau_8 \sim \frac{1}{A_{0\leftarrow 1}} = 26 \text{ sec} \quad . \tag{26}$$

At pressures greater than five torr, HI*(v=8) will undergo more than 3×10^8 collisions during τ_8.[29] Since only 10^5 collisions are needed to deactivate HI(v=1) (and HI*(v=8) should deactivate faster) fluorescence can be ignored.[30]

b) Collisional deactivation is therefore the important process for HI* relaxation. Deactivation cross sections have been measured for HI(v=1) and HI(v=2).[30-32] They are

$$\sigma_{HI(v=1)} = 0.0038 \text{ Å}^2 \tag{27}$$

$$\sigma_{HI(v=2)} = 0.046 \text{ Å}^2 \quad . \tag{28}$$

The relaxation of HI(v=1) can proceed only by a V→T,R process while HI(v=2) can also relax by a V→V transition. This dramatic increase in relaxation cross section going from equation 27 to equation 28 shows that the V→V process is much faster than the V→T,R in HI. This is true in general.[31] The V→V transition is therefore assumed to be the dominant relaxation process in HI*(v=8).

Unfortunately, equation 23 still does not help one solve equation 20 since k_E has not been measured either. However, if HI were a harmonic oscillator, then

$$k_{E\,(\text{harmonic})} = \frac{8k_F}{2} \quad , \tag{29}$$

where k_F refers to the measured reaction

$$HI(v=2) + HI(v=0) \rightarrow 2HI(v=1) \quad .^{33} \qquad (F)$$

HI, of course, is not a harmonic oscillator, thus equation 29 is not strictly valid. Indeed, the V→V transfer rate may be significantly slower than that predicted by equation 29 since the mechanical anharmonicity of HI prevents reaction E from being a resonant energy transfer process (see Table I). Since a better approximation is not available, we use equation 29, obtaining

$$k_D \sim 4k_F = 7.7 \times 10^5 \text{ torr}^{-1} \text{ sec}^{-1} \qquad (30)$$

This value of K_D is used in Appendix II to evaluate equation 20 for k_B. Under the experimental conditions cited there, it is required that

$$k_B \geq 7 \times 10^2 \text{ torr}^{-1} \text{ sec}^{-1}$$

in order to observe the vibrationally enhanced reaction.

An upper bound may be placed on k_B using data on k_A. If vibrational enhancement is important in reaction A as Anderson's experiment suggests,[34] the following mechanism may be proposed for the thermal reaction:

$$HI + HI \rightleftarrows HI^*(v=8) + HI \qquad (G)$$

$$HI^*(v=8) + HI \rightarrow H_2 + 2I \qquad (B)$$

Since reaction B proceeds slowly compared to the fast equilibrium

reaction G, a Boltzman distribution can be assumed. Using rate data for k_A,[4] an upper limit on k_B,

$$k_B \geq 2.7 \times 10^7 \text{ torr}^{-1} \text{ sec}^{-1}$$

may be set. This is an upper limit on k_B, since it was assumed that reactions G and B were the only source of thermally produced H_2.

It is seen that the experimental conditions proposed in Appendix II would allow one to measure this rate (provided that the transition frequency is known within the accuracy needed to tune the laser).

VII. Appendix I

Vibrational Photolysis of HI

A molecular beam study done by J. B. Anderson[34] showing that translational energy is unimportant in reaction A suggests that vibrational energy plays an important role in his reaction.

Continuum radiation (suitably filtered to prevent electronic excitation of HI) from a 2.5 kW xenon arc lamp (Hanovia 975 C-98) was focused into a photolysis vessel. The vessel, a 10 cm hollow quartz sphere, was gold plated on the exterior (except for the entrance window) to maximize the optical path. This vessel was mounted in a resistance heated oven whose temperature was regulated with a platinum resistance thermometer bridge (Hallikainen Thermotrol 1472 A). Temperature was measured with six iron constantan thermocouples placed around the sphere. A mercury-free vacuum line attached to the vessel was used to purify HI (Matheson, 98%) and transfer to the vessel. After photolysis, HI + I_2 from the reaction mixture were frozen over liquid nitrogen. The remaining H_2 was measured in a precalibrated mass spectrometer (C.E.C. 21-103 C). When the rate of H_2 formation was compared to that of a similarly thermostated but not irradiated vessel, it was discovered that the reaction rate in the photolyzed vessel was higher.

It is extremely important to note that the effect of vibrational energy on the reaction rate is not necessarily the difference between the rates of the irradiated and non-irradiated samples. Since the experiment was conducted in the gas phase rather than by crossed molecular beams, it

is quite possible that vibrationally excited HI, produced by multiquantum absorption, may be collisionally deactivated before reaction with another molecule, pumping rotational and translational energy into the system as well as vibrational energy. Thus, the experiment does not distinguish between a rate increase due to vibrational excitation and a rate increase due to heating effects which may be produced by the intense light source used in the photolysis. Because of this ambiguity, results of many recent experiments concerned with the rate of vibrational energy on reaction rate are questionable.[26]

Using the mechanism developed in the Discussion, equation 18 and equation 19 are obtained. If I_0 and ℓ are fixed, $\{HI^*\}_{ss}$ is constant. Equation 19 may be simplified to

$$Rate_{H_2} = k_B\{HI^*\}_{ss}\{HI\} + k_A\{HI\}^2 = k'\{HI\} + k_A\{HI\}^2 \quad . \quad (32)$$

According to equation 32, a plot of $Rate_{H_2}/\{HI\}$ should be a straight line of slope k_A and intercept k'. Results for the photolyzed samples are shown in Figures 8-13. Shown in Figures 14 and 15 are results for thermal samples. Notice that both sets of data (photolyzed and thermal) have non-zero intercepts. If the intercepts are plotted versus observed temperature, measured at the vessel wall, there appears to be a difference between the photolyzed and unphotolyzed results (see Figure 16).

Since the slope of the lines in Figures 8-15 is k_A, the well known thermal rate constant, an internal reaction temperature may be calculated from the Arrhenius expression for reaction A.[4] As shown in Table IV, temperatures calculated in this manner are between 8K and 20K higher than

Table IVa. Summary of HI Photochemistry.

Figure	Conditions (P = Photolyzed) (T = Thermal)	T_{obs} (K)	T_{calc} (K)	ΔT (K)
8	P	670.9	711.9	40.9
9	P	650.7	687.9	37.2
10	P	693.1	728.3	35.2
11	P	639.9	677.5	37.6
12	P	653.7	667.1	13.4
13	P	664.0	695.3	31.2
14	T	668.6	676.7	8.1
15	T	697.8	713.0	15.2

Table IVb. Summary of HI Photochemistry.

Figure	Conditions	k_A (liter mol^{-1} sec^{-1} x 10^{-4})		σ_{k_A}	k' (sec^{-1} x 10^{-7})		$\sigma_{k'}$
8	P	9.34	±	0.64	6.93	±	1.2
9	P	3.15	±	0.14	2.49	±	0.29
10	P	18.9	±	0.90	16.1	±	1.0
11	P	1.91	±	0.23	1.13	±	0.38
12	P	1.15	±	0.10	2.91	±	0.17
13	P	4.43	±	0.45	5.68	±	0.74
14	T	1.85	±	0.15	4.08	±	0.32
15	T	9.82	±	0.45	8.73	±	0.85

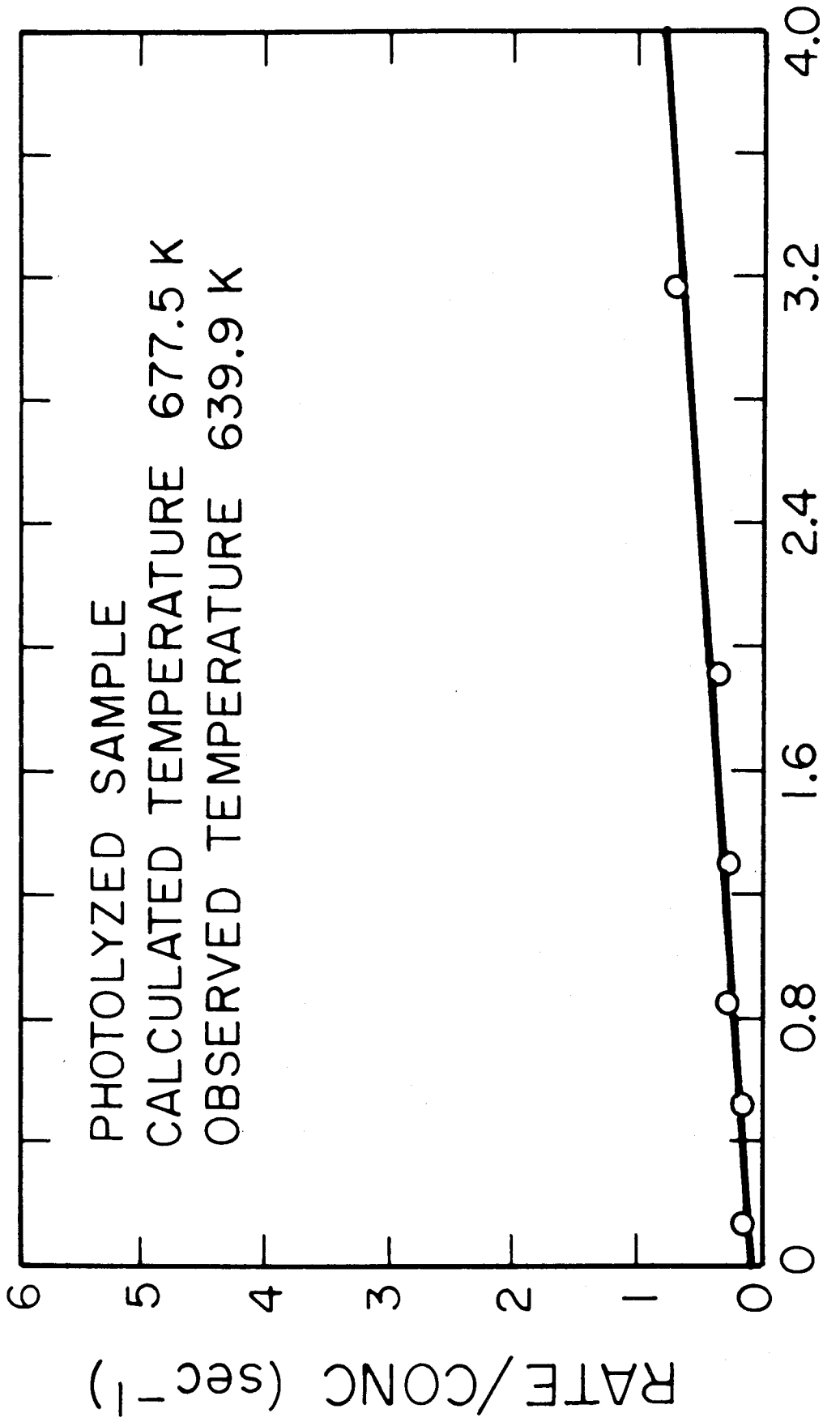
PHOTOLYZED SAMPLE
CALCULATED TEMPERATURE 677.5 K
OBSERVED TEMPERATURE 639.9 K
RATE/CONC (sec⁻¹)
CONCENTRATION (mol/liter) (x 10⁻³)
0
1
2
3
4
5
6
0
0.8
1.6
2.4
3.2
4.0

Figure 8

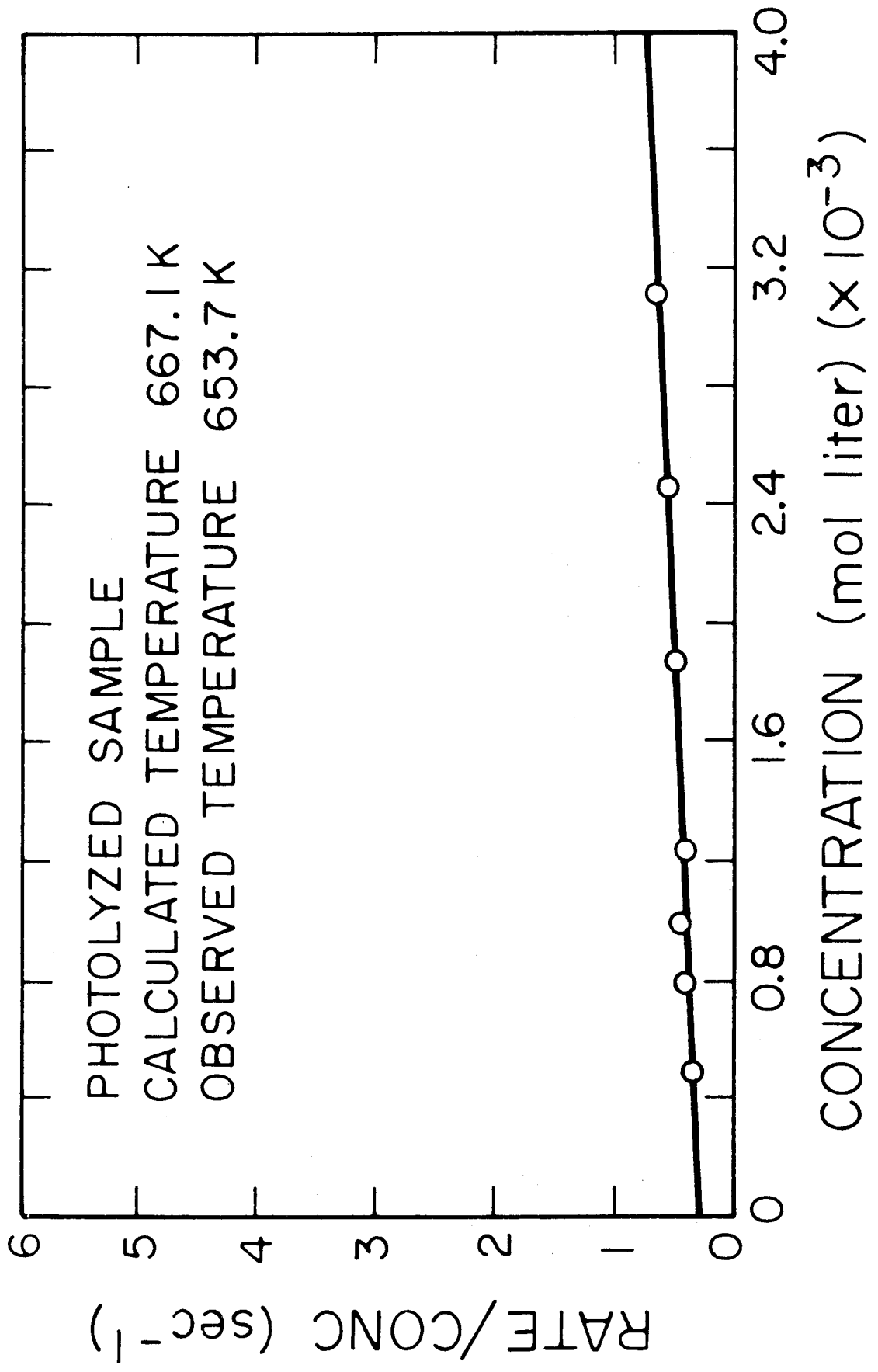
PHOTOLYZED SAMPLE
CALCULATED TEMPERATURE 667.1 K
OBSERVED TEMPERATURE 653.7 K
RATE/CONC (sec⁻¹)
CONCENTRATION (mol liter) (X 10⁻³)
0
1
2
3
4
5
6
0
0.8
1.6
2.4
3.2
4.0

Figure 9

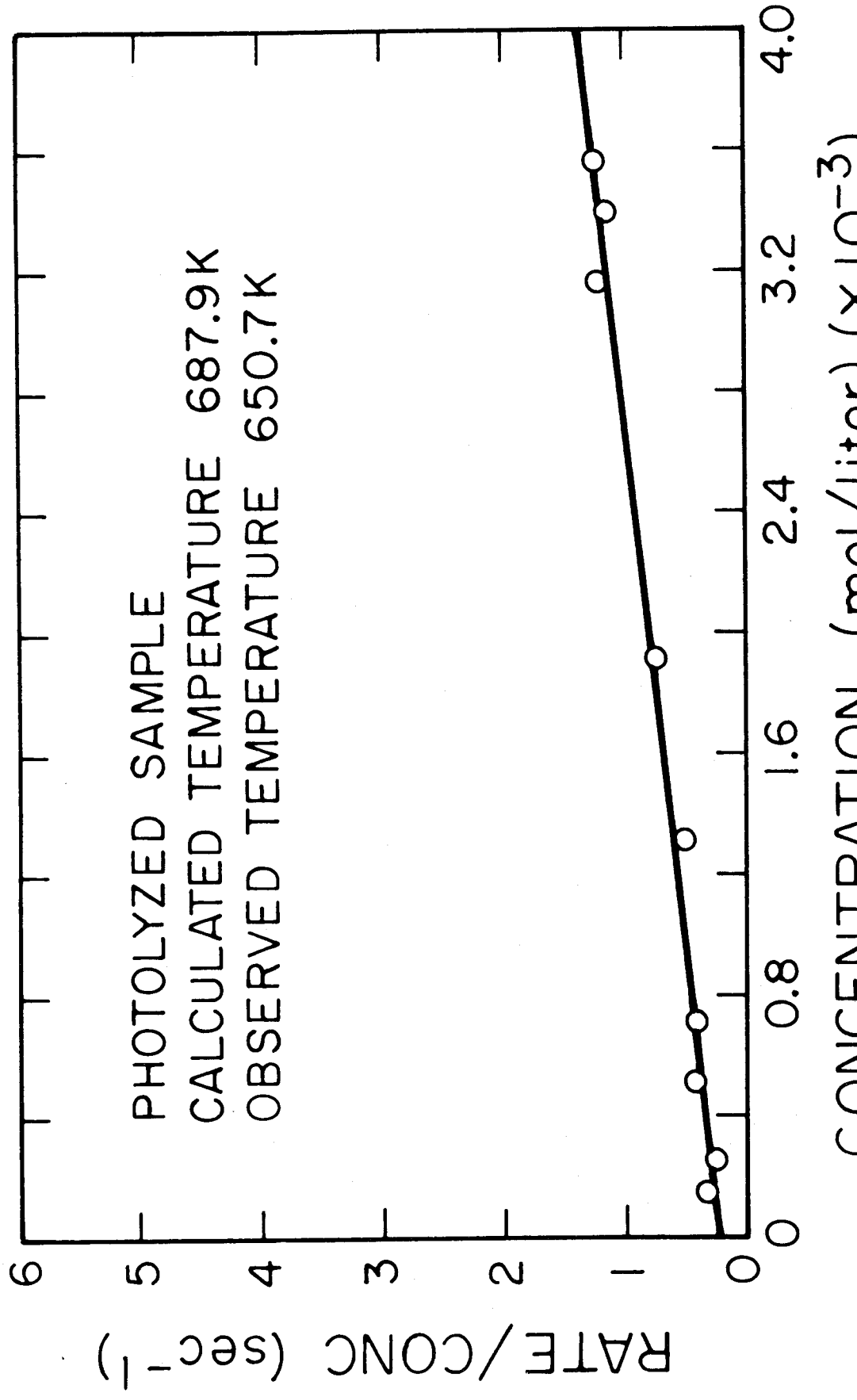
PHOTOLYZED SAMPLE
CALCULATED TEMPERATURE 687.9K
OBSERVED TEMPERATURE 650.7K
RATE/CONC (sec⁻¹)
CONCENTRATION (mol/liter) (x 10⁻³)
0
1
2
3
4
5
6
0.8
1.6
2.4
3.2
4.0

Figure 10

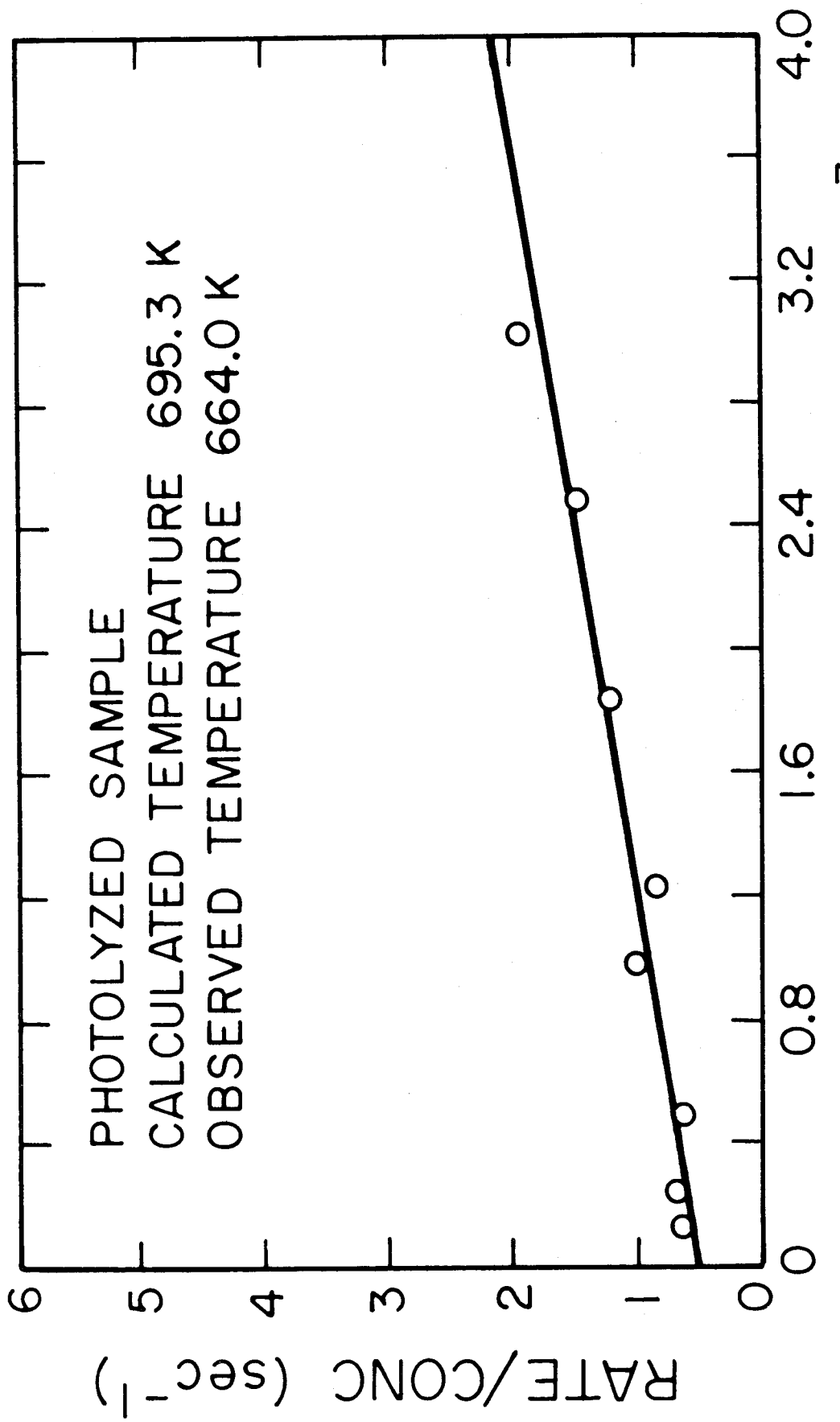
PHOTOLYZED SAMPLE
CALCULATED TEMPERATURE 695.3 K
OBSERVED TEMPERATURE 664.0 K
RATE/CONC (sec^{-1})
CONCENTRATION (mol/liter) (x 10^{-3})
0
1
2
3
4
5
6
0
0.8
1.6
2.4
3.2
4.0

Figure II

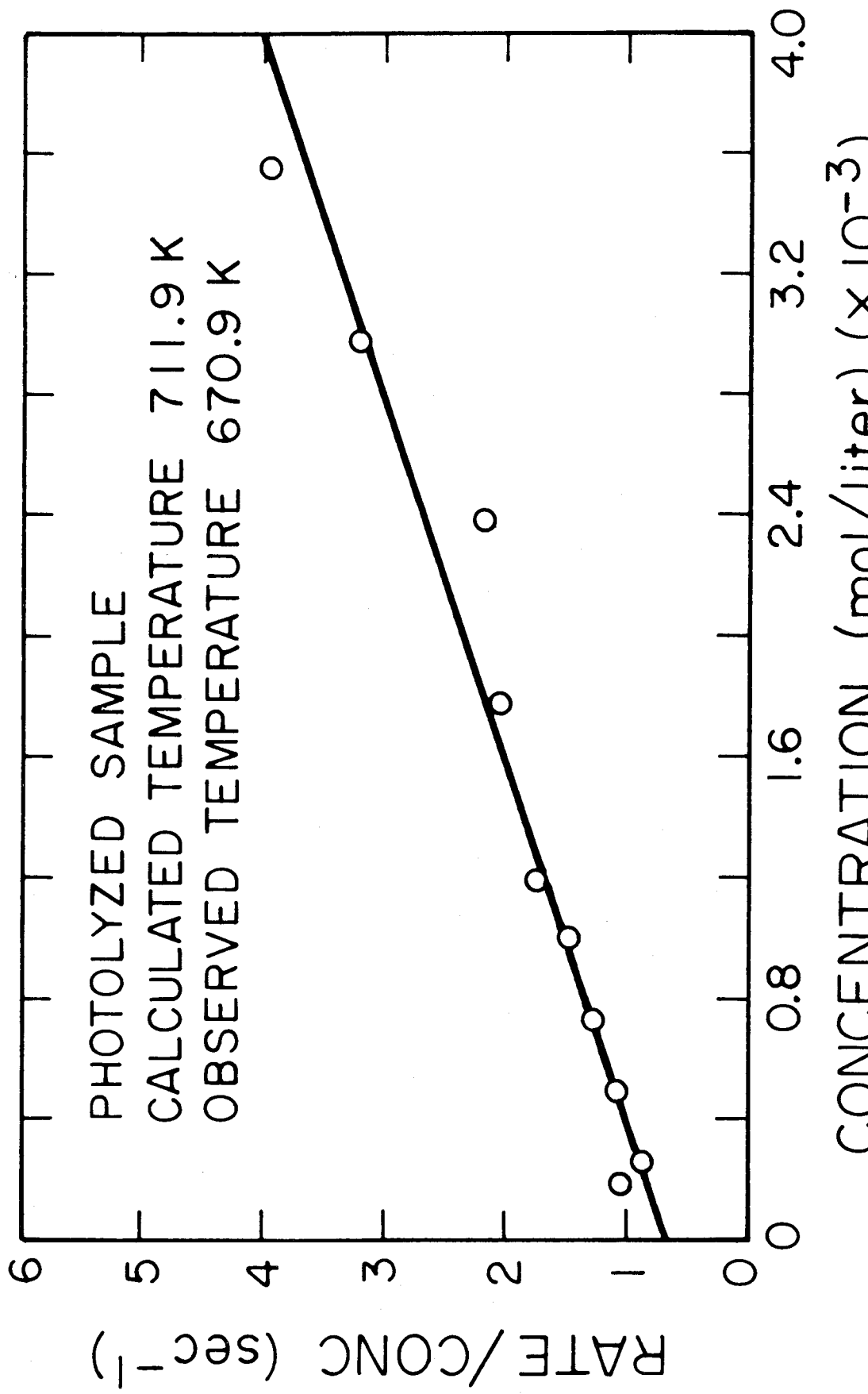
PHOTOLYZED SAMPLE
CALCULATED TEMPERATURE 711.9 K
OBSERVED TEMPERATURE 670.9 K
RATE/CONC (sec^{-1})
CONCENTRATION (mol/liter) (X 10^{-3})
0
1
2
3
4
5
6
0
0.8
1.6
2.4
3.2
4.0

Figure 12

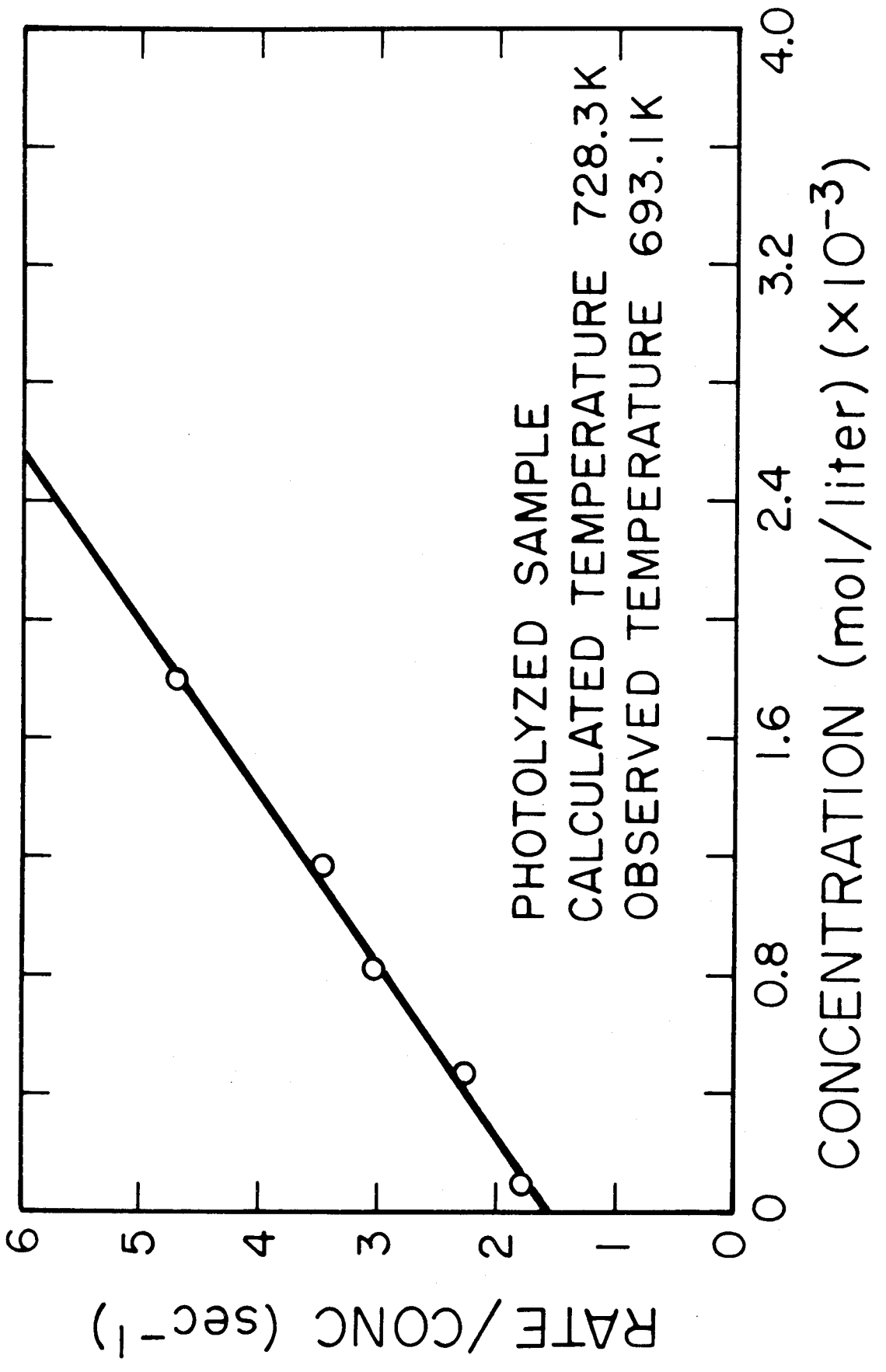
PHOTOLYZED SAMPLE
CALCULATED TEMPERATURE 728.3K
OBSERVED TEMPERATURE 693.1K
RATE/CONC (sec⁻¹)
CONCENTRATION (mol/liter) (×10⁻³)
0
1
2
3
4
5
6
0
0.8
1.6
2.4
3.2
4.0

Figure 13

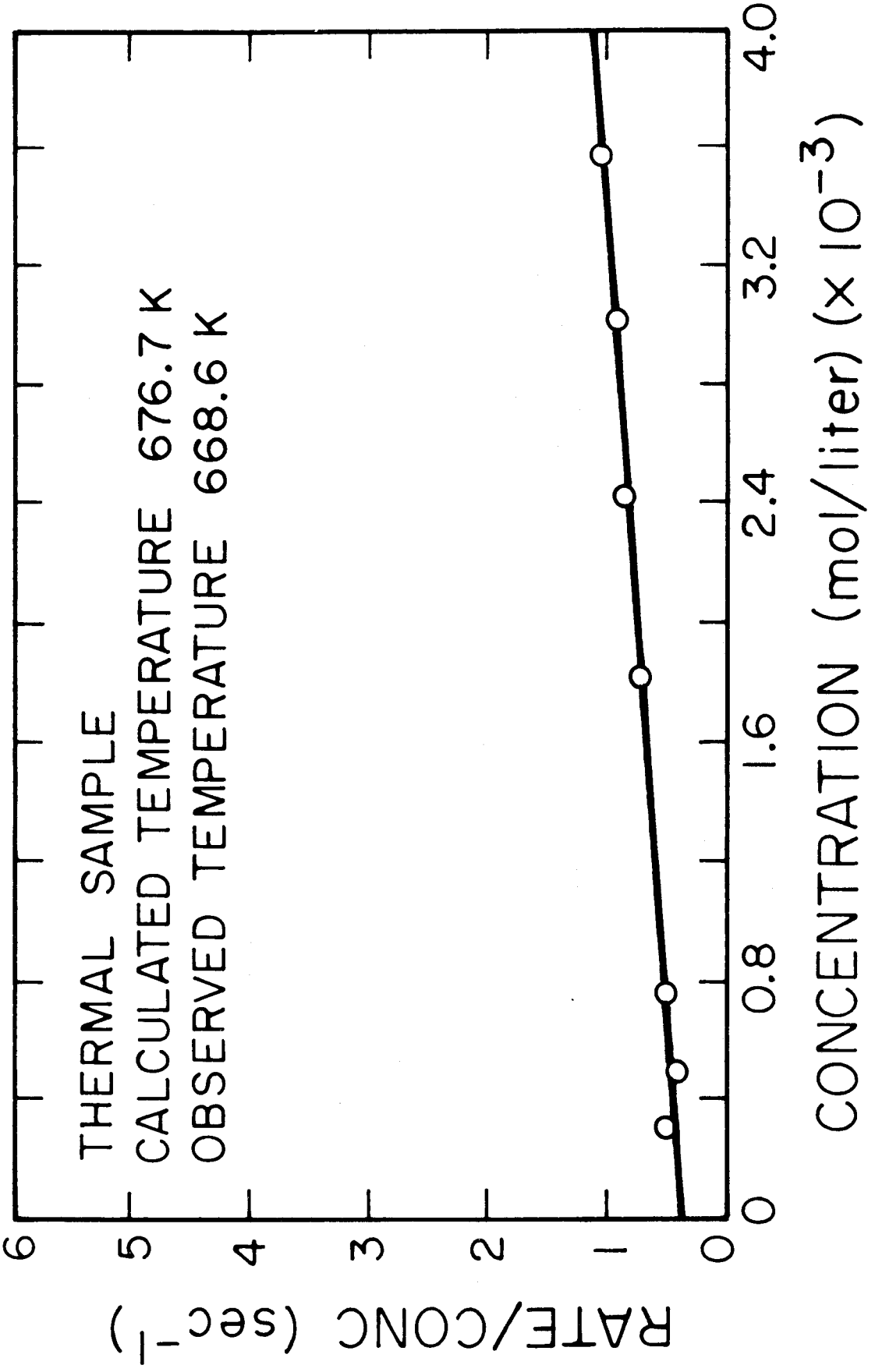
THERMAL SAMPLE
CALCULATED TEMPERATURE 676.7 K
OBSERVED TEMPERATURE 668.6 K
RATE/CONC (sec^{-1})
CONCENTRATION (mol/liter) (x 10^{-3})
0
1
2
3
4
5
6
0
0.8
1.6
2.4
3.2
4.0

Figure 14

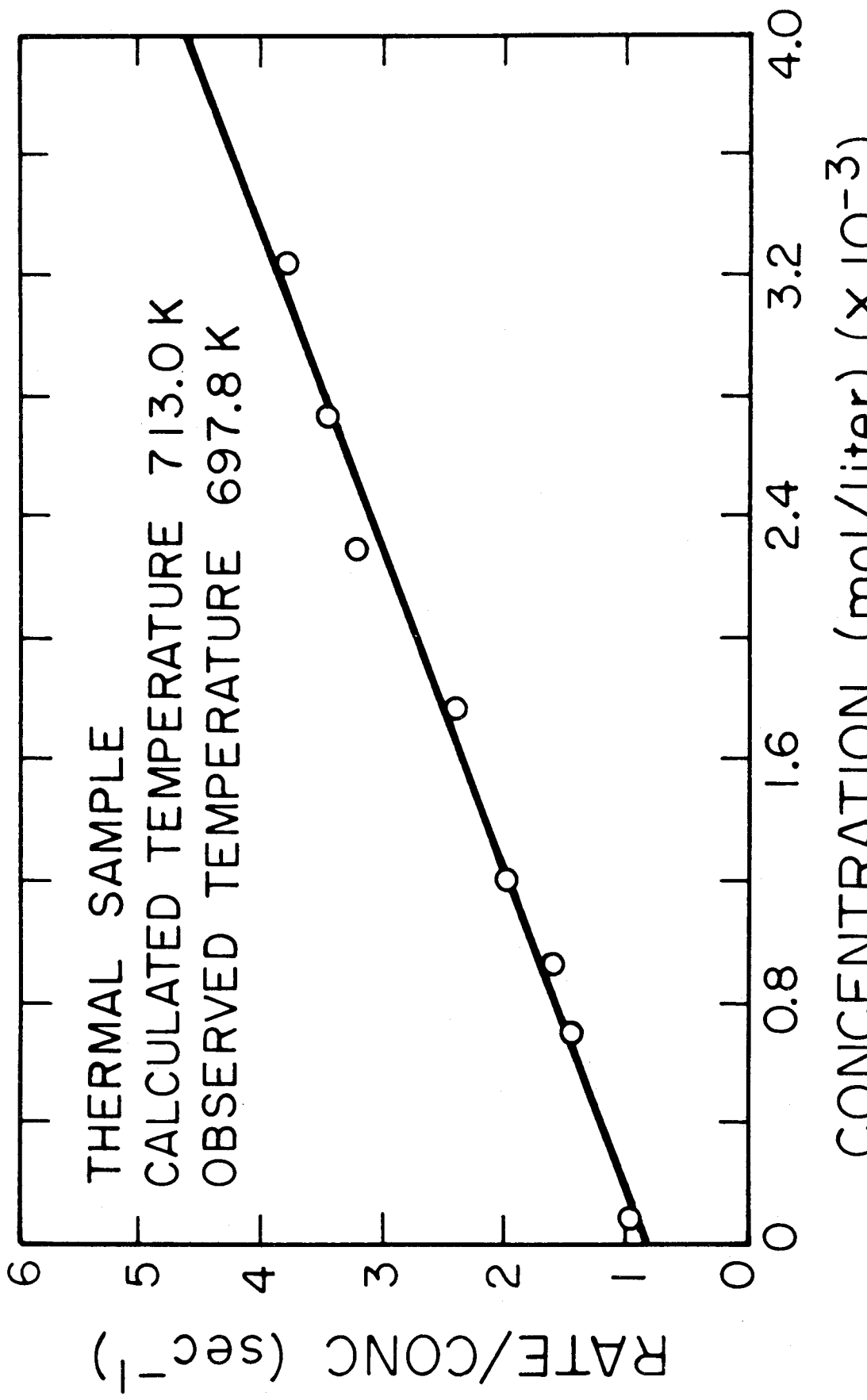
THERMAL SAMPLE
CALCULATED TEMPERATURE 713.0 K
OBSERVED TEMPERATURE 697.8 K
RATE/CONC (sec^{-1})
CONCENTRATION (mol/liter) (x 10^{-3})
0
1
2
3
4
5
6
0
0.8
1.6
2.4
3.2
4.0

Figure 15

Figure 16. The intercepts, k', from Figures 8-15 are plotted versus measured cell temperature.

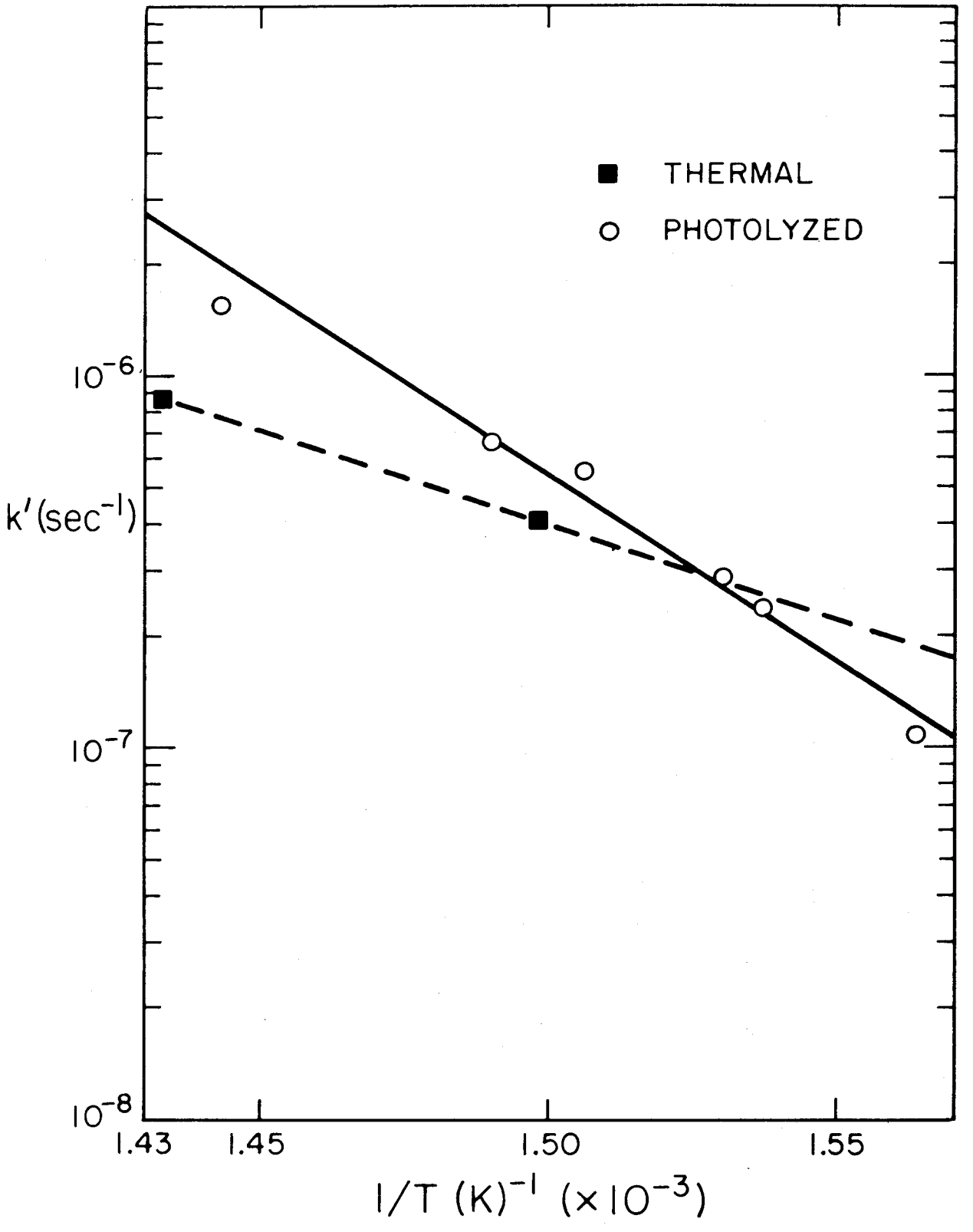
THERMAL
PHOTOLYZED
10^{-6}
10^{-7}
10^{-8}
k′(sec^{-1})
1.43
1.45
1.50
1.55
1/T (K)$^{-1}$ (×10^{-3})

those measured at the cell wall. If the intercepts in Figures 8-15 are shown in an Arrhenius plot using T calculated rather than T observed, it is immediately apparent that the observed rate increase in the photolyzed samples is not due to vibration excitation but is a heating effect (Figure 17).

The temperature dependence of k' seen in Figure 17 may be described by $k' = 2416 \times \exp(-30.93/RT)$. The origin of this first order thermal reaction component is unclear. Later experiments showed that H_2 envolved slowly from the walls of the quartz vessel. However, when quartz wool was added to the vessel, increasing the surface to volume ratio by 30, k' was unchanged. It is interesting to note that a similar non-zero intercept is seen in the thermal data of Crist and Taylor[4] when plotted as in Figure 8.

The procedure outlined in Appendix II can be used to evaluate equation 20 under the conditions of this experiment ($I_0 = 10^{13}$ photons sec^{-1} cm, ℓ = 100 cm). If $k_D \sim 7 \times 10^5$ $torr^{-1}$ sec^{-1}, the maximum rate of H_2 production would be 6×10^9 molecules/sec even if $k_B \to \infty$. This is well below the minimum detectible rate (3×10^{11} molecules/sec, see equation 34).

Figure 17. Figure 16 is replotted using the calculated reaction temperature (as explained in text).

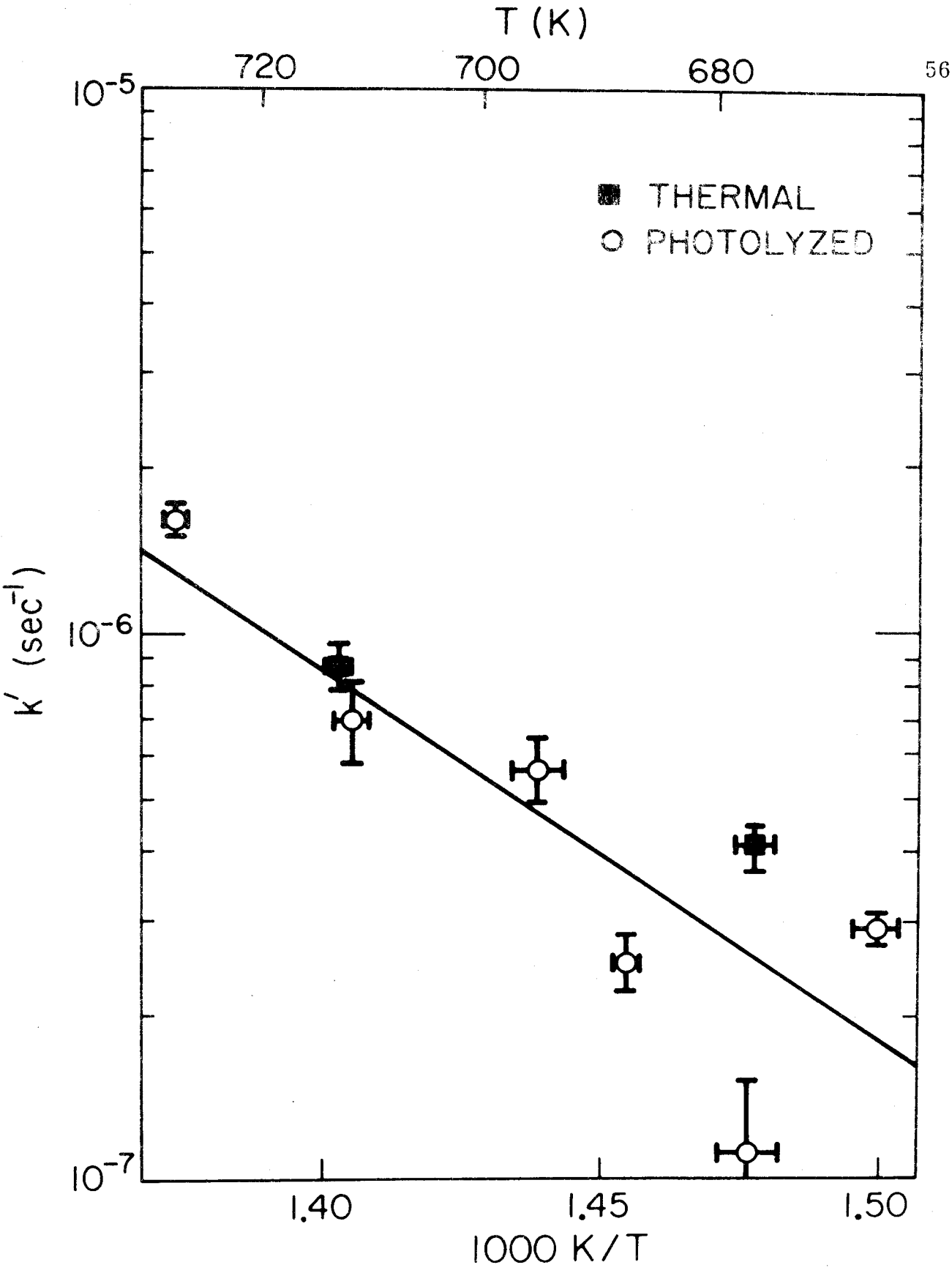
T (K)
720
700
680
10-5
10-6
10-7
k' (sec-1)
THERMAL
PHOTOLYZED
1.40
1.45
1.50
1000 K/T

VIII. Appendix II

Observation of Vibrational Excitation

Case i $\quad k_B < k_D \sim 7 \times 10^5$ torr^{-1} sec^{-1}

Choosing representative values of $I_0 = 10^{19}$ photons sec^{-1} cm (dye laser 3 watts, bandwidth 0.05 nm), $\ell = 50$ cm, and $\varepsilon_{HI} = 5 \times 10^{-5}$ atm^{-1} cm^{-2}, equation 19 yields a value for $\{HI^*\}_{ss}$,

$$\{HI^*\}_{ss} = 4.2 \times 10^7 \text{ molecules} \quad . \qquad (33)$$

The minimum number of H_2 molecules detectable by the mass spectrometer (C.E.C. 21-103C) is 3×10^{16} molecules. Using a reasonable photolysis time of 10^5 seconds (1.1 days), the minimum detectable rate of H_2 production is

$$\text{Rate} \geq 10^{11} \text{ molecules/sec} \quad . \qquad (34)$$

Equations 33 and 34 are used to solve equation 20 for k_B. Using $\{HI\} \sim 10$ torr, one finds that the minimum detectable value of k_B under the above experimental conditions is

$$k_B \geq 7 \times 10^2 \text{ torr}^{-1} \text{ sec}^{-1} \quad .$$

Case ii. $\quad k_B > k_D \sim 7 \times 10^5$ torr^{-1} sec^{-1}

Equation 22 may be used immediately to give

$$\text{Rate}_B \sim 3 \times 10^{14} \text{ molecules/sec} \quad . \qquad (35)$$

This is three orders of magnitude above the minimum detectable rate, equation 34.

IX. References

1. Truman J. Odiorne and Philip R. Brooks, J. Chem. Phys., 51, 4676 (1969).

2. Larry A. Pugh and K. Marahari Rao, J. Mol. Spectrosc., 37. 373 (1971).

3. John H. Sullivan, J. Chem. Phys., 46, 73 (1967).

4. Alfred H. Taylor, Jr. and R. H. Crist, J. Am. Chem. Soc., 65, 1377 (1941).

5. Leonard I. Schiff, Quantum Mechanics (McGraw-Hill Book Company, New York, New York, 1968) third ed., p. 403.

6. Gerhard Herzberg, Spectra of Diatomic Molecules (D. Van Nostrand, Inc., Princeton, New Jersey, 1950) second ed., pp. 19-21.

7. J. R. Oppenheimer, Proc. Camb. Phil. Soc., 23, 327 (1926).

8. R. E. Meredith and F. G. Smith, J. Quant. Spectrosc. Radiat. Transfer, 13, 89 (1973).

9. R. Herman, J. Mol. Spectros., 2, 369 (1958).

10. G. Herzberg, op. cit., p.540.

11. M. McClintock, W. Demtröder, and R. N. Zare, J. Chem. Phys., 51, 5509 (1969).

12. Claude Haeusler, Claude Meyer, and Pierre Barchewitz, J. Physique, 25, 961 (1964).

13. B. Rosen, Spectroscopic Data Relative to Diatomic Molecules (Pergamon Press, Oxford, England, 1970), p. 187.

14. G. Herzberg, op. cit., p. 99.

15. R. Jost and W. Kohn, Phys. Rev., 88, 382 (1952).

16. Bruce Carnahan, H. A. Luther, and James O. Wilkes, Applied Numerical Methods (John Wiley and Sons, New York, New York, 1969), p.267.

17. George Ameer and William Benesch, J. Chem. Phys., 37, 2699 (1962).

18. William Benesch, J. Chem. Phys., 39, 1048 (1963).

19. William S. Benedict, Robert Herman, Gordon E. Moore, and Shirleigh Silverman, J. Chem. Phys., 26, 1671 (1957).

20. J. M. Herbelin and G. Emanuel, Aerospace Report No. TR-0074 (4530)-5, Aerospace Corp., Los Angeles, California, 1974, p. 6.

21. J. Trischka and H. Salwen, J. Chem. Phys., 31, 218 (1959).

22. This has also been shown true for HF for $v \leq 10$. See R. J. Fallon, J. T. Vanderslice, and E. A. Mason, J. Chem. Phys., 32, 698 (1960).

23. John U. White, J. Opt. Soc. Am., 32, 285 (1942).

24. G. Herzberg, Nature, 163, 170 (1949).

25. H. J. Bernstein and G. Herzberg, J. Chem. Phys., 16, 30 (1948).

26. This point is evidently overlooked by many researchers in the field. See, for example, H. B. Kaplob and O. M. Ctel' max, J.E.T.P. Letters, 11, 135 (1970); M. Brunet and F. Boimer, C. R. Acad. Sci. (Paris), 271C, 1116 (1970); A. Yogev and J.R.M.J. Loewentein, J. Amer. Chem. Soc., 94, 1091 (1972).

27. This is calculated using $S_{0\to1} = 0.37$ atm^{-1} cm^{-2} and reference 6.

28. This is true, for HF, HCl, and probably true for HI. See reference 20, Table V.

29. A. Guthrie, Vacuum Technology (Wiley, New York, 1965), pp. 12, 505.

30. H. L. Chen, J. Chem. Phys., 55, 5551 (1971).

31. Measurements of V→T,R and V→V processes in HCl indicate that V→V reactions occur at least ten times faster than V→T,R. These results are typical of other molecules studied. See, for example, H. L. Chen, J. Chem. Phys., 54, 4072 (1971).

32. J. H. Ahl and T. A. Cool, J. Chem. Phys., 55, 1980 (1971).

33. N. Cohen, Aerospace Report No. TR-0073(3430)-9, Aerospace Corporation, Los Angeles, California, 1974, p. 48.

34. S. B. Jaffe and J. B. Anderson, J. Chem. Phys., 51, 1057 (1969).

35. B. Lunelli, J. A. Betts, and Aron Kuppermann, Annual Report: Chemistry and Chemical Engineering, Caltech, Pasadena, California, 1972, p. 58.